Localized mRNA translation mediates maturation of cytoplasmic cilia in *Drosophila* spermatogenesis

Short Running title: mRNA localization in sperm cilia maturation

Jaclyn M Fingerhut[1,2,*] and Yukiko M Yamashita[1,2,3,4,*]

[1]Cellular and Molecular Biology Program, [2]Life Sciences Institute, [3]Department of Cell and Developmental Biology, [4]Howard Hughes Medical Institute, University of Michigan, Ann Arbor, MI 48109, USA

* Correspondence: jaclynmf@umich.edu, yukikomy@umich.edu

Abstract

Cytoplasmic cilia, a specialized type of cilia in which the axoneme resides within the cytoplasm rather than within the ciliary compartment, are proposed to allow the efficient assembly of very long cilia. Despite being found diversely in male gametes (e.g. *Plasmodium* microgametocytes and human and *Drosophila* sperm), very little is known about cytoplasmic cilia assembly. Here we show that a novel RNP granule containing the mRNAs for axonemal dynein motor proteins becomes highly polarized to the distal end of the cilia during cytoplasmic ciliogenesis in *Drosophila* sperm. This allows for the localized translation of these axonemal dyneins and their incorporation into the axoneme directly from the cytoplasm. We found that this RNP granule contains the proteins Reptin and Pontin, loss of which perturbs granule formation and prevents incorporation of the axonemal dyneins, leading to sterility. We propose that cytoplasmic cilia require the local translation of key protein constituents such that these proteins are incorporated efficiently into the axoneme.

Author Summary

Cytoplasmic cilia, which are found in human and *Drosophila* sperm, are unique in that the axoneme is exposed to the cytoplasm. The authors show that a novel RNP granule containing axonemal dynein mRNAs facilitates localized translation of these axonemal proteins, facilitating cytoplasmic cilia formation.

Abbreviations

SC spermatocyte
IFT intraflagellar transport
ODA Outer dynein arm
IDA Inner dynein arm
RNP Ribonucleoprotein
smFISH single molecule RNA fluorescent in situ hybridization
IF Immunofluorescent
IC Individualization complex
TEM Transmission light microscopy

Introduction

Cilia are microtubule-based structures present on the surface of many cells. These specialized cellular compartments can be non-motile primary cilia that largely function in signaling, or motile cilia that can either move extracellular materials (e.g. lung multiciliated cells) or allow for cell motility (e.g. *Chlamydomonas* flagellum, sperm in many species) (Ishikawa and Marshall, 2011). It is well established that most cilia are separated from the bulk cytoplasm (Fig. 1 A), which serves to concentrate signaling molecules for rapid response to extracellular signals received by the cilia, and that the ciliary gate at the base of the cilia forms a diffusion barrier, through which molecules must be selectively transported (Reiter et al., 2012; Wheway et al., 2018). However, recent studies identified an additional type of cilia, called cytoplasmic cilia, in which the axoneme (the microtubule-based core of the cilia) is exposed to the cytoplasm (Fig. 1 A) (Avidor-Reiss et al., 2017; Avidor-Reiss and Leroux, 2015; Dawson and House, 2010; Fawcett et al., 1970; Sinden et al., 1976; Tates, 1971; Tokuyasu, 1975). Cytoplasmic cilia are found in human and *Drosophila* sperm as well as in *Plasmodium* and *Giardia*. There are two proposed advantages to cytoplasmic cilia: 1) faster assembly as the cell does not need to rely on ciliary transport mechanisms, allowing for the assembly of longer cilia, and 2) proximity to mitochondria for energy (Avidor-Reiss and Leroux, 2015; Sinden et al., 2010). Despite being found across diverse taxa, very little is known about how cytoplasmic cilia are assembled and whether their assembly bears similarity to that of traditional compartmentalized cilia (Desai et al., 2018).

Cytoplasmic ciliogenesis has been proposed to occur in two stages (Fig. 1 A) (Avidor-Reiss and Leroux, 2015). In the first stage, microtubules are polymerized in a small compartmentalized region, which is similar to canonical compartmentalized cilia, at the most distal end of the cilia (Gottardo et al., 2013; Tokuyasu, 1975). This region is gated by a transition zone (Caudron and Barral, 2009; Kwitny et al., 2010; Vieillard et al., 2016). This entire compartmentalized region, called the ciliary cap or the growing end, migrates away from the basal body, which is docked at the nuclear membrane (Basiri et al., 2014; Fawcett et al., 1970). The ciliary cap does not change in size as the cilia elongates. The continued polymerization of microtubules inside the ciliary cap displaces recently synthesized microtubules out of the compartmentalized region, exposing them to the cytoplasm (Fig. 1 A). The second stage is axoneme maturation, in which additional axonemal proteins (e.g.

axonemal dyneins, the motor proteins that confer motility by allowing axonemal microtubules to slide against each other, Fig. 1 B) are added to the bare microtubule structure after it emerges from the ciliary cap (Tates, 1971; Tokuyasu, 1975). Axoneme maturation was inferred to occur in the cytoplasm based on the dispensability of ciliary transport mechanisms and the inefficiency of relaying on diffusion through the transition zone (Avidor-Reiss and Leroux, 2015; Breslow et al., 2013; Briggs et al., 2004; Han et al., 2003; Hoeng et al., 2008; Kee et al., 2012; Lin et al., 2013; Sarpal et al., 2003). However, how this maturation process occurs in the cytoplasmic compartment to allow for cytoplasmic cilia formation remains unknown.

Drosophila spermatogenesis provides an excellent model for the study of cytoplasmic ciliogenesis (Fig. 1 B), owing to rich cytological knowledge of spermatogenesis and the conservation of almost all known ciliary proteins (Zur Lage et al., 2019). Developing spermatids elongate from 15μm to 1,900μm (1.9mm) (Tates, 1971; Tokuyasu, 1975). Within mature sperm, the cytoplasmic cilia are 1,800μm and the ciliary caps (the compartmentalized region) are only ~2μm. Ciliogenesis starts in premeiotic spermatocytes (SCs), which assemble short primary (compartmentalized) cilia (Fabian and Brill, 2012; Gottardo et al., 2013; Riparbelli et al., 2012; Tates, 1971). Prior to axoneme elongation, these primary cilia, which were docked at the plasma membrane in SCs, invaginate, forming the ciliary cap. During axoneme elongation, the majority of the length of the cilia will be exposed to the cytoplasm, as described above. Accordingly, axoneme assembly in *Drosophila* does not require intraflagellar transport (IFT) (Han et al., 2003; Sarpal et al., 2003), the process used by traditional compartmentalized cilia to ferry axonemal proteins from the cytoplasm into the ciliary compartment for incorporation (Rosenbaum and Witman, 2002). Other cytoplasmic cilia have been found not to require IFT for their assembly (Avidor-Reiss and Leroux, 2015; Briggs et al., 2004; Hoeng et al., 2008), leading to the appreciation of a distinct type of cilia: based on the dispensability of IFT, it was postulated that axoneme maturation must occur in the cytoplasm, hence the term ‘cytoplasmic cilia’.

It has long been known that SCs transcribe almost all genes whose protein products are needed post-meiotically and that these mRNAs may not be translated until days later when proteins are needed (Barckmann et al., 2013; Olivieri and Olivieri, 1965). We previously showed that the Y-linked testis-specific axonemal dynein heavy chain genes *kl-3*

and *kl-5*, as well as the testis-specific axonemal dynein intermediate chain *Dic61B*, are transcribed in SCs (Fingerhut et al., 2019). However, axoneme elongation does not begin until after meiosis, suggesting that these mRNAs may not be translated until later in development. Intriguingly, we previously showed that *kl-3* and *kl-5* mRNAs localize to cytoplasmic granules in SCs. Ribonucleoprotein (RNP) granules (e.g. stress granules, P granules and germ granules) are known to play critical roles in mRNA regulation, such as mediating the subcellular localization of mRNAs and controlling the timing of translation (Anderson and Kedersha, 2009; Buchan, 2014; Medioni et al., 2012). Therefore, we decided to investigate the role of this novel RNA granule in the translational regulatory mechanisms that ensure proper axoneme assembly and found that it plays an essential role in the incorporation of axonemal proteins, providing the first insights into the molecular mechanism of cytoplasmic cilia maturation. We show four axonemal dynein heavy chain mRNAs, including *kl-3* and *kl-5*, colocalize in these novel granules in late SCs along with the AAA+ (ATPases Associated with diverse cellular Activities) proteins Reptin (Rept) and Pontin (Pont). These RNP granules are segregated during the meiotic divisions and localize to the distal end of the cytoplasmic compartment as the axoneme elongates during spermiogenesis. We further show that Rept and Pont are required for RNP granule formation, and that RNP granule formation is necessary for robust translation and incorporation of the axonemal dynein proteins into the axoneme. We propose that cytoplasmic cilia maturation relies on the local translation of axonemal components such that they can be incorporated into the bare microtubule structure as it emerges from the ciliary cap.

Results

Axonemal dynein heavy chain mRNAs colocalize in RNP granules in spermatocytes

In our previous study, we analyzed the expression of the Y-linked axonemal dynein genes *kl-3* and *kl-5* and showed that these two mRNAs localized to cytoplasmic granules in late SCs (Fingerhut et al., 2019). Using single molecule RNA fluorescent *in situ* hybridization (smFISH), we found that mRNAs for four testis-specific axonemal dynein heavy chain genes (the Y-chromosome genes *kl-2*, *kl-3*, and *kl-5*, as well as the autosomal gene *Dhc98D* (Carvalho et al., 2000; Goldstein et al., 1982; Hardy et al., 1981; Zur Lage et al., 2019))

colocalize together within RNP granules in the cytoplasm of late SCs, with each SC containing several of these cytoplasmic granules (Fig. 1 C and D). We termed these granules "kl-granules" after the three Y-linked constituent mRNAs. It should be noted that robust transcription of these genes is still ongoing in SC nuclei (visible as bright nuclear signal, Fig. 1 C and D) but these are nascent transcripts that still contain intronic RNA, whereas the kl-granules in the cytoplasm do not contain intronic RNA, as we showed previously (Fingerhut et al., 2019). The present study focuses the fate of these cytoplasmic RNPs that contain mature mRNA. mRNAs within a kl-granule are spatially sub-organized: *kl-3* and *kl-5* mRNAs, which encode outer dynein arm (ODA) dynein heavy chain proteins, cluster together in the core of the kl-granule while *kl-2* and *Dhc98D* mRNAs, which encode inner dynein arm (IDA) dynein heavy chain proteins, localize peripherally (Fig. 1 E – G). This is similar to the sub-compartmentalization observed in other RNP granules, including the germ granules in the *Drosophila* ovary, stress granules, P granules and nucleoli (Boisvert et al., 2007; Jain et al., 2016; Trcek et al., 2015; Wang et al., 2014). We noted that kl-granule formation is unlikely to be dependent upon any one mRNA constituent as RNAi mediated knockdown of *kl-3*, *kl-5*, *kl-2*, or *Dhc98D* (*bam-gal4>UAS-kl-3*$^{TRiP.HMC03546}$ or *bam-gal4>UAS-kl-5*$^{TRiP.HMC03747}$ or *bam-gal4>UAS-kl-2*^{GC8807} or *bam-gal4>UAS-Dhc98D*$^{TRiP.HMC06494}$) did not perturb granule formation despite efficient knockdown (Fig. S1).

We conclude that mRNAs for the testis-specific axonemal dynein heavy chains localize to novel RNP granules, which we termed kl-granules, in late SCs.

The kl-granules segregate during the meiotic divisions and localize to the distal end of elongating spermatids

As the kl-granules contain mRNAs for axonemal proteins that are only necessary for spermiogenesis, we next followed the fate of the kl-granules through meiosis and into spermiogenesis. The kl-granules segregate through the two sequential meiotic divisions (Fig. 2 A) such that each resulting haploid spermatid receives a relatively equal amount of kl-granule (Fig. 2 B). Upon completion of meiosis, the resultant spermatids are interconnected due to incomplete cytokinesis during the four mitotic divisions that occur early in germ cell development and the two meiotic divisions, forming a cyst of 64 spermatids (Fuller, 1993; Hime et al., 1996). As the axoneme starts to elongate within each spermatid, the nuclei

cluster to the proximal end of the cyst while the axoneme elongates unidirectionally away from the nuclei with the ciliary caps clustered at the distal end of the cyst (Fig. 1 B) (Fabian and Brill, 2012). Strikingly, we found that the kl-granules become localized to the distal end of elongating spermatid cysts (Fig. 2 C). This polarized localization remains as the axoneme continues to elongate (Fig. 2 D and E). At later stages of elongation, the kl-granules begin to dissociate and the mRNAs become more diffusely localized at the distal end (Fig. 2 D and E). Interestingly, some mRNAs dissociate from the kl-granules before others: *kl-3* and *kl-5* mRNAs (encoding ODA proteins) dissociate earlier than *kl-2* and *Dhc98D* mRNAs (encoding IDA proteins) (Fig. 2 D and F). It is of note that the differential timing of dissociation correlates with the sub-compartmentalization of constituent mRNAs described above: *kl-3* and *kl-5* localize to the core of the kl-granules and dissociate first (Fig. 1 E), whereas *kl-2* and *Dhc98D* localize to the periphery of the kl-granules (Fig. 1 F) and dissociate later. These results show that kl-granules exhibit stereotypical localization to the growing end of spermatids after being segregated during meiosis, implying that programmed positioning of the kl-granules may play an important role during spermatid elongation and axoneme maturation.

The AAA+ proteins Reptin and Pontin colocalize with the kl-granules

To further understand how kl-granules form and their potential function, we sought to identify a protein(s) that localize to the kl-granules. In our previous study, we screened for proteins involved in the expression of the Y-linked axonemal dynein genes (Fingerhut et al., 2019). Reptin (Rept) and Pontin (Pont), two AAA+ proteins (Puchades et al., 2020), were included in this screen because of their high expression in the testis and their involvement in RNP complex formation in other systems (Mao and Houry, 2017; Robinson et al., 2013). Also, studies in *Drosophila*, mouse, zebrafish, *Chlamydomonas* and Xenopus have specifically implicated Rept and Pont in axoneme/motile cilia assembly and/or sperm motility, although the underlying mechanism remains unknown (Dafinger et al., 2018; Huizar et al., 2018; Li et al., 2017; Stolc et al., 2005; Tammana and Tammana, 2017; Zhao et al., 2013; Zur Lage et al., 2018).

We found that Rept and Pont colocalize in cytoplasmic granules in SCs through elongating spermatids (Fig. 3 A and B). Immunofluorescent staining combined with smFISH

(IF-smFISH) showed that Rept and Pont colocalize with the kl-granules. Pont first colocalizes with *Dhc98D* mRNA in early SCs (Fig. 3 C) and with all other kl-granule constituent mRNAs in later SCs (Fig. 3 D) and throughout spermatid elongation (Fig. 3 E). Close examination of the kl-granules in late SCs revealed that Pont is not evenly distributed within a kl-granule and rather concentrates near the core with *kl-3* and *kl-5* mRNAs (Fig. 1 E and Fig. 3 F). In contrast, *kl-2* and *Dhc98D* mRNAs occupy the periphery of the kl-granule (Fig. 1 F), where Pont is less concentrated.

We conclude that Rept and Pont localize to the kl-granules together with axonemal dynein heavy chain mRNAs. It is interesting to note that previous studies have proposed that Rept and Pont function as chaperones in the assembly of axonemal dynein motors (complexes containing a combination of dynein heavy, intermediate, and light chains) (Huizar et al., 2018; Li et al., 2017; Zur Lage et al., 2018). It remains unknown whether previously reported Rept- and Pont-containing chaperon complexes also contain mRNA (see Discussion).

Reptin and Pontin are required for kl-granule assembly

To explore the function of Rept and Pont in kl-granule formation, we performed RNAi mediated knockdown of either *rept* or *pont* (*bam-gal4>UAS-rept*^{KK105732} or *bam-gal4>UAS-pont*^{KK101103}). In addition to eliminating the targeted protein, depletion of *rept* resulted in loss of Pont and vice versa, reminiscent of findings from previous studies, likely because these proteins stabilize each other as components of the same complex (Fig. S2) (Gorynia et al., 2011; Li et al., 2017; Rivera-Calzada et al., 2017; Venteicher et al., 2008).

We next determined whether Rept and Pont are needed for kl-granule assembly. Indeed, knockdown of *rept* or *pont* resulted in disruption of the kl-granules. smFISH clearly detected the presence of dispersed *kl-3* and *kl-5* mRNAs in late SCs, suggesting that *rept* and *pont* are required for kl-granule formation but not for the stability of the constituent mRNAs (Fig. 4 A – C, note that nuclear signal was oversaturated in order to focus on the dispersed cytoplasmic signal). This effect was more pronounced in elongating spermatids where *kl-3* and *kl-5* mRNAs were diffuse throughout the entire cyst in the RNAi conditions (Fig. 4 D – F). RT-qPCR confirmed that mRNA levels were not reduced compared to cross-sibling controls (Fig. 4 G and H), demonstrating that kl-granule formation is not required for mRNA stability.

This is in accordance with observations in other systems that suggest that RNA granule formation is not required for mRNA stability and may be more important for mRNA localization or translation (Bley et al., 2015; Lee et al., 2020).

Interestingly, knockdown of *rept* or *pont* had a somewhat different effect on *kl-2* and *Dhc98D* mRNAs. smFISH for *kl-2* and *Dhc98D* following RNAi of either *rept* or *pont* showed loss of kl-granule localization in late SCs similar to that seen for *kl-3* and *kl-5* (Fig. 4 I – K). However, in elongating spermatids, *kl-2* and *Dhc98D* mRNAs appeared to localize properly at the distal end of the cyst (Fig. 4 L – N). Considering that Pont primarily colocalized with *kl-3* and *kl-5* mRNAs (Fig. 3 F), this may suggest that other proteins participate in localizing *kl-2* and *Dhc98D* mRNAs to the kl-granule.

In conclusion, Rept and Pont are critical for assembling the kl-granules.

kl-granule assembly is required for efficient Kl-3 translation and sperm motility

Previous studies in *Drosophila* and mouse demonstrated that Rept and Pont are required for male fertility (Li et al., 2017; Zur Lage et al., 2018). We confirmed that seminal vesicles, where mature motile sperm are stored after exiting the testis, were empty in *rept* or *pont* RNAi testes (Fig. 5 A – C), as was observed for *kl-3*, *kl-5*, *kl-2*, or *Dhc98D* RNAi testes (Fig. S3) (Fingerhut et al., 2019; Zur Lage et al., 2018).

We further characterized the sterility phenotype of *rept* and *pont* RNAi testes and found that spermiogenesis fails during individualization. As sperm develop as cysts, the process of individualization removes excess cytoplasm from the spermatids and separates the cyst into individual sperm via actin-rich individualization complexes (ICs) (Fabian and Brill, 2012). The ICs form around the nuclei at the proximal end of the cyst and progress evenly towards the distal end (Fig. 5 D). It is well established that defects in axoneme assembly, including loss of axonemal dynein motor proteins, perturb IC progression (Fatima, 2011; Fingerhut et al., 2019; Wang et al., 2019). We found that RNAi-mediated knockdown of *rept* or *pont*, does not affect IC assembly but does result in disorganized IC progression (Fig. 5 E – J), as is observed following knockdown of *kl-3*, *kl-5*, *kl-2*, or *Dhc98D* (Fig. S3) (Fingerhut et al., 2019).

As previous studies have implicated Rept and Pont in male fertility and axonemal dynein motor assembly, and the observed individualization defects are characteristic of

axonemal defects, we analyzed Kl-3 protein levels following *rept* or *pont* RNAi. Western blotting using total testis extracts revealed that Kl-3 protein levels are drastically reduced following knockdown of *rept* or *pont* (Fig. 5 K). Taken together, our results demonstrate that Rept and Pont are required for mRNAs to congress in the kl-granule, which in turn is required for efficient translation. This defect in axonemal dynein expression is the likely cause of sterility in *rept* and *pont* RNAi testes.

kl-granule formation and localization are required for cytoplasmic cilia maturation

Precise mRNA localization and localized translation are widely utilized mechanisms to ensure that proteins are concentrated where they are needed (Glock et al., 2017; Medioni et al., 2012). As described above, the kl-granules localize to the distal end of elongating spermatids (Fig. 2) where bare axonemal microtubules are first exposed to the cytoplasm after being displaced from the ciliary cap as new microtubules are polymerized. We therefore postulated that the kl-granule may function in cytoplasmic cilia maturation. We first determined whether the kl-granules localize within the ciliary cap or within the cytoplasmic compartment. By using Unc-GFP to mark the ring centriole, a structure at the base of the ciliary cap at the boundary between the cytoplasmic and compartmentalized regions (Baker et al., 2004; Phillips, 1970), we found that the kl-granules are located within the cytoplasmic compartment, immediately proximal to the ciliary cap (Fig. 6 A), suggesting that this may be the site of localized Kl-3 translation. Indeed, we not only found that FLAG-tagged Kl-3 protein (expressed from the endogenous locus, see Methods) occupies the same region proximal to the ciliary cap as the kl-granules but that Kl-3 protein is restricted to the cytoplasmic compartment while the microtubules extend into the compartmentalized compartment (i.e. the ciliary cap) (Fig. 6 B). These results indicate that while the axonemal microtubules are polymerized within the ciliary cap, axoneme maturation (the incorporation of axonemal dyneins and other axonemal proteins) may occur within the cytoplasmic compartment, as has been proposed (Avidor-Reiss and Leroux, 2015).

Detailed examination of Kl-3 protein within the elongating spermatid cysts provided insights into where Kl-3 protein may be translated and incorporated into the growing axoneme (Fig. 6 C and D). At the distal end of the cyst, where the kl-granules are concentrated, Kl-3 protein was predominantly observed in the cytoplasm, while being

excluded from the axonemal microtubules (Fig. 6D, see the right panel for intensity plot showing mutually exclusive localization of microtubules and Kl-3). This suggests that Kl-3 protein at the distal end may represent the pool of newly translated Kl-3 before it is incorporated into the axoneme, which is also consistent with the presence of kl-granules at this location. In contrast to the distal end, Kl-3 protein was observed to colocalize with axonemal microtubules at the proximal end (Fig. 6D, see the right panel for intensity plot showing colocalization of microtubules and Kl-3), suggesting that Kl-3 protein has been successfully incorporated into the axoneme. These results suggest that Kl-3 protein is translated at the distal end, where the kl-granules localize, and that the diffuse cytoplasmic Kl-3 protein is the newly synthesized pool, which is subsequently incorporated into the axoneme.

Following RNAi mediated knockdown of *rept* or *pont*, which prevents kl-granule formation (Fig. 4) and drastically reduces Kl-3 protein levels (Fig. 5 K), we still observed Kl-3 protein in the cytoplasm at the distal end (Fig. 6 F and H), although at a much reduced level. However, Kl-3 protein was never observed to colocalize with the axonemal microtubules at the proximal end upon *rept* or *pont* RNAi (Fig. 6 E and G), suggesting that Rept and Pont are required for incorporation of Kl-3 into the axoneme.

Consistent with this notion, transmission electron microscopy (TEM) revealed that the ODAs and IDAs are largely absent from the axonemes following *rept* or *pont* RNAi. (Fig. 6 I – K). Additional gross axonemal defects (e.g. broken axonemes) were present in the RNAi conditions (Fig. 6 L – N), suggesting additional impairments to axoneme assembly. These results suggest that localized mRNA translation via formation of the kl-granules is required for axonemal dynein motor proteins to incorporate into the axoneme.

Discussion

Cytoplasmic cilia have been found in organisms as diverse as *Plasmodium* and humans (Avidor-Reiss et al., 2017; Avidor-Reiss and Leroux, 2015; Dawson and House, 2010; Fawcett et al., 1970; Sinden et al., 1976; Tates, 1971; Tokuyasu, 1975). While it has been proposed that axoneme maturation proceeds through the direct incorporation of axonemal proteins from the cytoplasm, this model remained untested (Avidor-Reiss and Leroux, 2015). Our study provides the first insights into the mechanism of cytoplasmic cilia

342 formation. Our results show that localized translation of axonemal dynein mRNAs facilitates
343 the maturation of cytoplasmic cilia by allowing for the efficient incorporation of axonemal
344 dynein proteins into bare axonemal microtubules directly from the cytoplasm.
345
346 **Mechanism for cytoplasmic cilia maturation**
347 It has been proposed that cytoplasmic cilia assemble in two steps (Avidor-Reiss and
348 Leroux, 2015): first, microtubules are polymerized within a small compartmentalized region
349 of the cilia, then, as the bare microtubules are displaced from this region, axonemal proteins
350 are incorporated directly from the cytoplasm during the maturation step. Previous studies
351 that have shown that IFT, the process used by traditional compartmentalized cilia to ferry
352 axonemal proteins into the ciliary compartment, is dispensable for *Drosophila*
353 spermiogenesis, and that the genomes of some other organisms known to form cytoplasmic
354 cilia (e.g. *Plasmodium*) do not encode IFT and/or transition zone proteins (Avidor-Reiss and
355 Leroux, 2015; Breslow et al., 2013; Briggs et al., 2004; Han et al., 2003; Hoeng et al., 2008;
356 Kee et al., 2012; Lin et al., 2013; Sarpal et al., 2003). These studies led to the notion that
357 maturation of cytoplasmic cilia ought to happen in the cytoplasm, although direct evidence
358 has been lacking.
359 Our study, which identified a novel RNP granule, the kl-granule, composed of
360 axonemal dynein heavy chain mRNAs and the proteins Rept and Pont, provides the first
361 molecular insights into cytoplasmic cilia maturation. Our results show that axonemal dynein
362 heavy chain mRNAs (*kl-3*, *kl-5*, *kl-2*, and *Dhc98D*) congress into kl-granules in SCs. We further
363 show that Rept and Pont are required for kl-granule assembly and the proper translation of
364 axonemal dynein mRNAs. We demonstrate that the polarized localization of kl-granule
365 mRNAs within the cytoplasmic compartment promotes localized translation and allows for
366 the incorporation of their encoded proteins into the axoneme, facilitating the maturation
367 step in cytoplasmic cilia assembly (Fig. 7). Our results refine the proposed two step model
368 for cytoplasmic cilia assembly by demonstrating that concentrating axonemal proteins
369 within distal regions of the cytoplasm is critical for maturation. Thus, axoneme maturation
370 proceeds in a stepwise fashion, allowing for the efficient assembly of this very long cilia. This
371 model implies that the proximal region of the axoneme should be more mature than the
372 distal region, a notion that is supported by previous studies that looked at axoneme

ultrastructure and tubulin dynamics within the axoneme (Noguchi et al., 2011; Sinden et al., 2010; Tokuyasu, 1975).

Function of Reptin and Pontin in dynein assembly

A wide range of functions have been assigned to Rept- and Pont-containing complexes including roles in chromatin remodeling, transcription regulation, DNA repair and ribosome assembly (Mao and Houry, 2017). They can act alone, together or as part of larger complexes (Huen et al., 2010; Kakihara and Saeki, 2014). Among these, previous studies have proposed that Rept and Pont are dynein arm preassembly factors – chaperones that take individual dynein motor subunits (i.e. the heavy, intermediate, and light chain proteins) and stabilize and assemble them into a motor unit in the cytoplasm that is then ferried into the cilia for incorporation (Desai et al., 2018; Fabczak and Osinka, 2019; Fowkes and Mitchell, 1998). These assembly factors include R2TP and R2TP-like complexes (which include Rept (RUVBL2) and Pont (RUVBL1)) in association with dynein axonemal assembly factors (DNAAFs) (Fabczak and Osinka, 2019). While previous studies have clearly demonstrated that Rept, Pont, R2TP, and DNAAFs are needed for axonemal dynein protein stability and incorporation (Huizar et al., 2018; Li et al., 2017; Liu et al., 2019; Yamaguchi et al., 2018; Zhao et al., 2013; Zur Lage et al., 2018), our study is the first to demonstrate involvement of axonemal dynein mRNAs with these complexes, showing that Rept and Pont are required for axonemal dynein mRNAs to localize to the kl-granules. It remains unknown whether the Rept- and Pont-associated dynein arm preassembly complexes reported in previous studies also contain dynein mRNAs. However, important differences exist between these preassembly complexes and the kl-granules. Firstly, while *kl-3* mRNA is present in the kl-granules, no puncta are observed for Kl-3 protein, indicating that Kl-3 protein does not concentrate within the kl-granules (or another granule) as dyneins do in the dynein preassembly complexes reported in other systems (Dafinger et al., 2018; Huizar et al., 2018). Additionally, dynein preassembly complexes were found to contain proteins (e.g. Wdr78 (Huizar et al., 2018)), where the *Drosophila* homolog (*Dic61B*) mRNAs are not constituents of the kl-granules (Fig. S4, see below). Therefore, the kl-granule may be a novel adaptation of a Rept and Pont containing dynein arm assembly complex specifically found in cytoplasmic cilia and is distinct from its role as a dynein preassembly factor in other systems.

It is likely that additional protein components of the kl-granule remain to be discovered. Structural analyses in previous studies have identified mechanisms by which other proteins interact with Rept and Pont (Rivera-Calzada et al., 2017), however, Rept and Pont do not have any RNA binding domains (Mao and Houry, 2017). Therefore, it is likely that additional proteins, not Rept and Pont themselves, physically interact with constituent mRNAs for kl-granule formation. Our data also supports the existence of additional proteins governing kl-granule dynamics. For example, as spermatids elongate, the ODA and IDA mRNAs separate slightly from each other while remaining polarized at the distal end (Fig. 2). Moreover, in the absence of Rept and Pont, the IDA mRNAs are still able to congress at the distal end of the elongating spermatid cyst, after failing to form kl-granules in SCs. In contrast, localization of the ODA mRNAs entirely depends on Rept and Pont, as ODA mRNAs remain diffuse throughout spermatogenesis following *rept* or *pont* RNAi. Finally, Pont more strongly colocalizes with the ODA mRNAs within the kl-granule (Fig. 3 F), which altogether suggests that there are additional proteins that can sort and specify the fate of these kl-granule mRNAs both alongside or in the absence of Rept and Pont. The identity of these additional proteins is the subject of further study. In addition, determining the involvement of the other dynein arm preassembly factors is of particular interest, especially considering the existence of multiple dynein arm assembly complexes that have been shown to differentially regulate IDA and ODA assembly (Fabczak and Osinka, 2019; Yamaguchi et al., 2018). It is also appealing to posit the existence of testis-specific factors which may help to distinguish the role of Rept and Pont in cytoplasmic cilia formation from its role in the assembly of other cellular bodies.

Purpose of mRNA localization to kl-granules

Interestingly, we found that not all mRNAs for axonemal/spermiogenesis proteins localize to the kl-granules (Fig. S4). mRNAs for other axonemal proteins (the dynein intermediate chain *Dic61B*, the dynein heavy chain *CG3339*, and the ODA docking complex component *CG17083* (Zur Lage et al., 2019)) as well as mRNAs for other Y-linked transcripts (*CCY* and *PPR-Y* (Carvalho et al., 2001)) and a non-axonemal spermatid protein (*fzo* (Hales and Fuller, 1997)) did not localize to the kl-granules. Instead they remain evenly distributed throughout the SC cytoplasm, despite also being important for sperm maturation (Fig. S4).

Additionally, we previously reported that mRNAs for the Y-liked gene *ORY* also gather in cytoplasmic RNA granules in late SCs (Fingerhut et al., 2019), however, these RNA granules are distinct from the kl-granule (Fig. S4 G).

In particular, it is intriguing that mRNA for *Dic61B*, an IDA intermediate chain that needs to bind to the IDA heavy chains Kl-2 and Dhc98D, is located differently (diffusely) within the spermatid cyst. Dynein preassembly is believed to be important for dynein protein stability and a prerequisite for axonemal incorporation (Fabczak and Osinka, 2019; Fowkes and Mitchell, 1998). An intriguing possibility is that temporal/spatial regulation of dynein mRNAs plays a role in helping the ordered assembly of dynein complexes. It will be of future interest to determine when and where during spermiogenesis dynein complexes are formed in the cytoplasmic cilia as well as what factors are necessary for their formation. A comprehensive understanding of kl-granule mRNAs and proteins would allow for further study into this temporal/spatial regulatory mechanism and a more thorough understanding of how the kl-granules function in the maturation of cytoplasmic cilia.

In summary, our study provides the first insights into the mechanism of cytoplasmic cilia maturation: mRNAs for axonemal dynein motor proteins are localized at the distal end of the axoneme within the cytoplasmic compartment, which allows for efficient maturation of cytoplasmic cilia through localized translation.

Materials and Methods

Fly husbandry

All fly stocks were raised on standard Bloomington medium at 25°C, and young flies (1- to 5-day-old adults) were used for all experiments. Flies used for wildtype experiments were the standard lab wildtype strain *yw* (y^1w^1). The following fly stocks were used: *bam-GAL4:VP16* (BDSC:80579), *UAS-kl-3*$^{TRiP.HMC03546}$ (BDSC:53317), *UAS-kl-5*$^{TRiP.HMC03747}$ (BDSC:55609), *UAS-Dhc98D*$^{TRiP.HMC06494}$ (BDSC:77181), and C(1)RM/C(1;Y)6, $y^1w^1f^1$/0 (BDSC:9460) were obtained from the Bloomington Stock Center (BDSC). *UAS-kl-2*^{GC8807} (VDRC:v19181), *UAS-rept*^{KK105732} (VDRC:v103483), and *UAS-pont*^{KK101103} (VDRC:v105408) were obtained from the Vienna *Drosophila* Resource Center (VDRC). *unc-GFP* (GFP-tagged *unc* expressed by the endogenous promoter) and Ub-α-tubulin84B-GFP were a gift of

Cayentano Gonzalez (Baker et al., 2004; Rebollo et al., 2004) and *bam-gal4* was a gift of Dennis McKearin (Chen and McKearin, 2003). The *kl-3-FLAG* strain was constructed using CRISPR mediated knock-in of a 3X-FLAG tag at the C-terminus of *kl-3* as previously described (Fingerhut et al., 2019).

Single molecule RNA fluorescent *in situ* hybridization

All solutions used for RNA FISH were RNase free. Testes from 2-3 day old flies were dissected in 1X PBS and fixed in 4% formaldehyde in 1X PBS for 30 minutes. Then testes were washed briefly in 1X PBS and permeabilized in 70% ethanol overnight at 4°C. Testes were briefly rinsed with wash buffer (2X saline-sodium citrate (SSC), 10% formamide) and then hybridized overnight at 37°C in hybridization buffer (2X SSC, 10% dextran sulfate (Sigma, D8906), 1mg/mL E. coli tRNA (Sigma, R8759), 2mM Vanadyl Ribonucleoside complex (NEB S142), 0.5% bovine serum albumin (BSA, Ambion, AM2618), 10% formamide). Following hybridization, samples were washed three times in wash buffer for 20 minutes each at 37°C and mounted in VECTASHIELD with DAPI (Vector Labs). Images were acquired using an upright Leica TCS SP8 confocal microscope with a 63X oil immersion objective lens (NA = 1.4) and processed using Adobe Photoshop and ImageJ software.
Fluorescently labeled probes were added to the hybridization buffer to a final concentration of 100nM. Probes against *kl-3*, *kl-5*, *kl-2*, *Dhc98D*, *CG3339*, *Dic61B*, *CG17083*, *CCY, PPR-Y*, *ORY* and *fzo* mRNAs were designed using the Stellaris® RNA FISH Probe Designer (Biosearch Technologies, Inc.) available online at www.biosearchtech.com/stellarisdesigner. Each set of custom Stellaris® RNA FISH probes was labeled with Quasar 670, Quasar 570 or Fluorescein (Table S1).

For strains expressing GFP (e.g. unc-GFP or Ub-α-tubulin84B-GFP), the overnight permeabilization in 70% ethanol was omitted.

Immunofluorescence staining

Testes were dissected in 1X PBS, transferred to 4% formaldehyde in 1X PBS and fixed for 30 minutes. Testes were then washed in 1X PBST (PBS containing 0.1% Triton-X) for at least 60 minutes followed by incubation with primary antibodies diluted in 1X PBST with

3% BSA at 4°C overnight. Samples were washed for at least 1 hour in 1X PBST, incubated with secondary antibody in 1X PBST with 3% BSA at 4°C overnight, washed as above, and mounted in VECTASHIELD with DAPI (Vector Labs). Images were acquired using an upright Leica TCS SP8 confocal microscope with a 63X oil immersion objective lens (NA = 1.4) and processed using Adobe Photoshop and ImageJ software.

The following primary antibodies were used: anti–α-tubulin (1:100; mouse, Sigma-Aldrich T6199), anti-FLAG (1:500; rabbit, Invitrogen PA1-984B), anti-Reptin (1:200; rabbit, gift of Andrew Saurin (Diop et al., 2008)), anti-Pontin (1:200; guinea pig, this study), Phalloidin-Alexa546 or 488 (1:200; ThermoFisher A22283 or A12379). The Pontin antibody was generated by injecting a peptide (CKVNGRNQISKDDIEDVH, targeting 18aa from the c terminal end of Pontin) in guinea pigs (Covance). Alexa Fluor-conjugated secondary antibodies (Life Technologies) were used at a dilution of 1:200.

A modified version of Stefanini's fixative (4% formaldehyde, 0.18% w/v Picric Acid (Ricca Chemical 5860), 0.3M PIPES pH7.5 (Alfa Aesar J63617), 0.05% Tween-20) was used in order to detect Kl-3 (Muller, 2008). No signal was detectable using traditional formaldehyde fixation.

Immunofluorescence staining with single molecule RNA fluorescent *in situ* hybridization

To combine immunofluorescent staining with smFISH, testes from 2-3 day old flies were dissected in 1X PBS and fixed in 4% formaldehyde in 1X PBS for 30 minutes. Then testes were washed briefly in PBS and permeabilized in 70% ethanol overnight at 4°C (unless from a strain expressing GFP, in which case this step was omitted). Testes were then washed with 1X PBS and blocked for 30 minutes at 37°C in blocking buffer (1X PBS, 0.05% BSA, 50μg/mL E. coli tRNA, 10mM Vanadyl Ribonucleoside complex, 0.2% Tween-20). Primary antibodies were diluted in blocking buffer and incubated at 4°C overnight. The testes were washed with 1X PBS containing 0.2% Tween-20, re-blocked for 5 minutes at 37°C in blocking buffer and incubated 4°C overnight in blocking buffer containing secondary antibodies. Then testes were washed with 1X PBS containing 0.2% Tween-20 and re-fixed for 10 minutes before continuing the smFISH starting from the brief rinse with wash buffer.

526

527 **RT-qPCR**

528 Total RNA from testes (50 pairs/sample) was extracted using TRIzol (Invitrogen)
529 according to the manufacturer's instructions. 1µg of total RNA was reverse transcribed using
530 SuperScript III® Reverse Transcriptase (Invitrogen) followed by qPCR using *Power* SYBR
531 Green reagent (Applied Biosystems) on a QuantStudio 6 Real-Time PCR system (Applied
532 Biosystems). Primers for qPCR were designed to amplify only mRNA. The genes analyzed by
533 qPCR are all predicted to contain megabase sized introns, and primers were designed to span
534 these large introns such that a product would be detect only if the intron had been spliced
535 out (Fingerhut et al., 2019). Relative expression levels were normalized to GAPDH and cross-
536 sibling controls. All reactions were done in technical triplicates with at least two biological
537 replicates. Graphical representation was inclusive of all replicates. Primers used are listed in
538 Table S1.

539

540 **Western blot**

541 Testes (40 pairs/sample) were dissected in Schneider's media at room temperature
542 within 30 minutes, the media was removed and the samples were frozen at -80°C until use.
543 After thawing, testes were then lysed in 200uL of 2X Laemmli Sample Buffer + βME (BioRad
544 161-0737). For Kl-3, samples were separated on a NuPAGE Tris-Acetate gel (3-8%, 1.5mm,
545 Invitrogen) and for Rept and Pont, samples were separated on a Novex Tris-Glycine gel
546 (10%, 1mm, Invitrogen) with the appropriate running buffer in a Xcell SureLock mini-cell
547 electrophoresis system (Invitrogen). For Kl-3, proteins were transferred using the XCell II
548 blot module (Invitrogen) onto polyvinylidene fluoride (PVDF) membrane (Immobilon-P,
549 Millipore) using NuPAGE transfer buffer (Invitrogen) without added methanol. For Rept and
550 Pont, transfer buffer contained 20% methanol. Membranes were blocked in 1X TBST (0.1%
551 Tween-20) containing 5% nonfat milk, followed by incubation with primary antibodies
552 diluted in 1X TBST containing 5% nonfat milk. Membranes were washed with 1X TBST,
553 followed by incubation with secondary antibodies diluted in 1X TBST containing 5% nonfat
554 milk. After washing with 1X TBST, detection was performed using the Pierce® ECL Western
555 Blotting Substrate enhanced chemiluminescence system (Thermo Scientific). Primary
556 antibodies used were anti–α-tubulin (1:2,000; mouse, Sigma-Aldrich T6199), anti-FLAG

(1:2,500; mouse, Sigma-Aldrich F1804), anti-Reptin (1:2000; rabbit, gift of Andrew Saurin), anti-Pontin (1:2000; guinea pig, this study), anti-Vasa (1:3000; rabbit, Santa Cruz Biotechnology D-260). The secondary antibodies were horseradish peroxidase (HRP) conjugated goat anti-mouse IgG, anti-rabbit IgG, or anti-guinea pig IgG (1:10,000; Abcam).

Phase contrast microscopy

Seminal vesicles were dissected in 1X PBS and transferred to slides for live observation by phase contrast on a Leica DM5000B microscope with a 40X objective (NA = 0.75) and imaged with a QImaging Retiga 2000R Fast 1394 Mono Cooled camera. Images were adjusted in Adobe Photoshop.

Transmission electron microscopy

Testes were fixed for one hour or overnight (at 4°C) with 2.5% glutaraldehyde in 0.1M Sorensen's buffer, pH7.4. Samples were rinsed twice for 5 minutes each with 0.1 M Sorensen's buffer and post fixed for one hour in 1 % osmium tetroxide in 0.1 M Sorensen's buffer. Next, testes were rinsed twice in double distilled water for 5 minutes each and *en bloc* stained with 2 % uranyl acetate in double distilled water for one hour. The samples were them dehydrated in increasing concentrations of ethanol, rinsed with acetone, and embedded in Epon epoxy resin. Thin sections were mounted on Formvar/carbon-coated slotted grids and post-stained with uranyl acetate and lead citrate. Samples were examined on a JEOL1400 transmission electron microscope and images captured using a sCMOS XR401 custom engineered optic camera by AMT (Advanced Microscopy Techniques Corp.).

Online supplemental material

Fig. S1 shows efficiency of RNAi knockdown of *kl-3*, *kl-5*, *kl-2*, and *Dhc98D* by smFISH and lack of dependence upon a single one of those transcripts for kl-granule formation (related to Fig. 1). Fig. S2 shows that RNAi of *rept* or *pont* results in efficient knockdown of both (related to Fig. 4). Fig. S3 shows the sterility phenotype of *kl-3*, *kl-5*, *kl-2*, and *Dhc98D* RNAi flies (related to Fig. 5). Fig. S4 shows smFISH for other axonemal, Y-linked, and spermatid-essential transcripts (related to Discussion).

Acknowledgements

We thank Drs. Dennis McKearin, Cayentano Gonzalez, and Andrew Saurin, the Bloomington Stock Center, and the Vienna *Drosophila* Resource Center for reagents. We thank Sasha Meshinchi and the University of Michigan Microscopy Core for help with EM experiments. We thank the Yamashita laboratory and Drs. Sue Hammoud and Joshua Bembenek for discussion and comments on the manuscript, Drs. Tomer Avidor-Reiss and Tony Mahowald for helpful suggestions, and Dr. Jiandie Lin for sharing equipment. This work was supported by the Howard Hughes Medical Institute (to YMY) and the NIH Cellular and Molecular Biology Training Grant T32-GM007315 (to JMF). The authors declare no competing financial interests.

Author Contributions: J.M. Fingerhut conceived the project and conducted experiments. J.M. Fingerhut and Y.M. Yamashita designed experiments, analyzed the data, and wrote the manuscript.

Figures

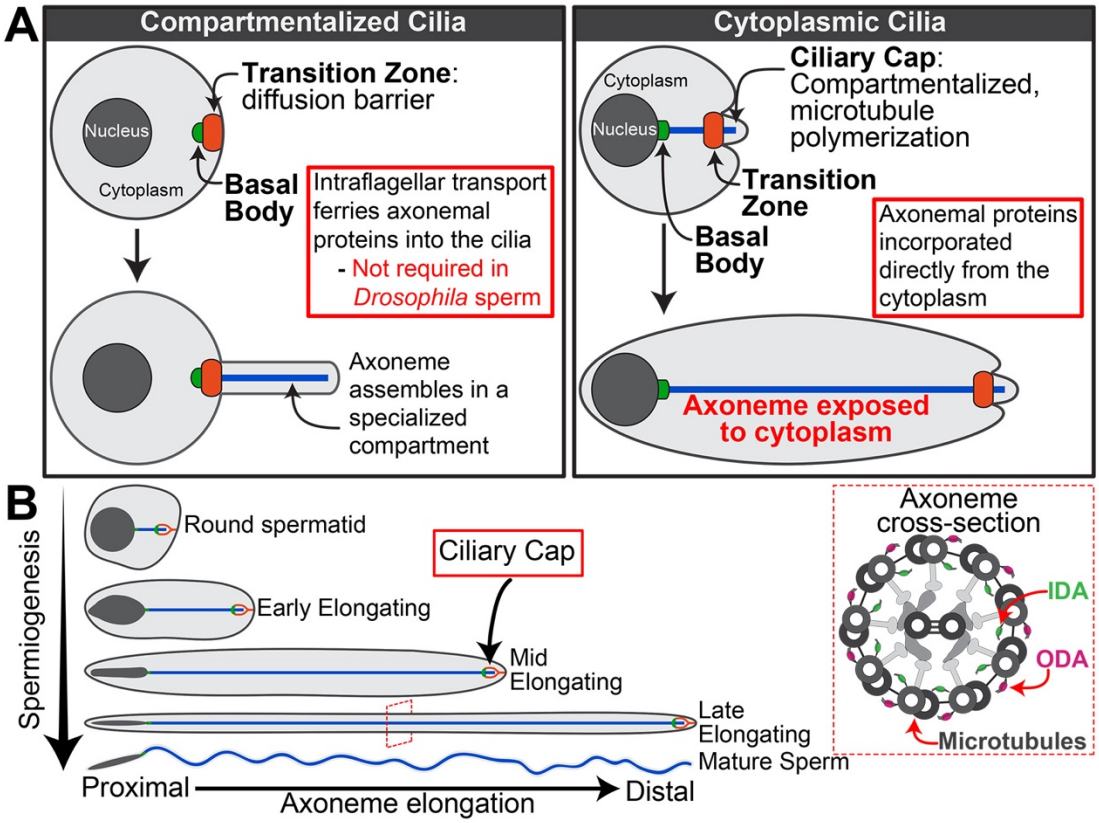

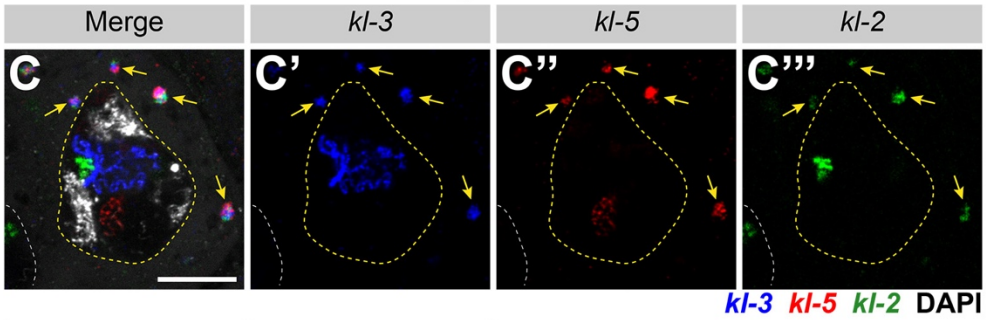

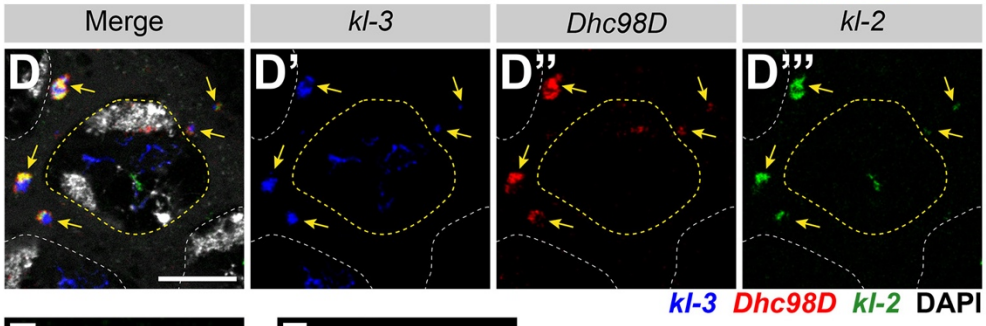

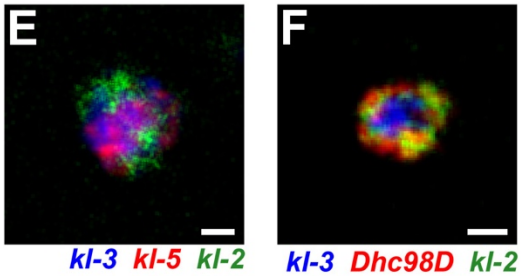

G

Gene	Function	Location
kl-3	Axonemal dynein heavy chain	ODA
kl-5		ODA
kl-2		IDA
Dhc98D		IDA

605

606 **Figure 1: Axonemal dynein heavy chain mRNAs colocalize in an RNP granule in**
607 **spermatocytes.**
608 **(A)** Diagram comparing and contrasting traditional compartmentalized cilia and
609 cytoplasmic cilia. Nucleus (dark gray), cytoplasm (light gray), basal body (green), transition
610 zone (orange) and axoneme (blue). **(B)** Diagram of *Drosophila* spermiogenesis with stages of
611 spermatid elongation. Nucleus (dark gray), cytoplasm (light gray), basal body & ring
612 centriole (green), ciliary cap (orange) and axoneme (blue). Axoneme cross section image
613 showing location of axonemal dynein arms. Microtubules and other structural components
614 (gray), inner dynein arm (green) and outer dynein arm (magenta). **(C and D)** smFISH against
615 axonemal dynein heavy chain transcripts in SCs showing *kl-3*, *kl-5*, and *kl-2* mRNAs (C) or *kl-*
616 *3*, *kl-2*, and *Dhc98D* mRNAs (D) in kl-granules. *kl-3* (blue), *kl-2* (green), *kl-5* (red, C), *Dhc98D*
617 (red, D), DAPI (white), kl-granules (yellow arrows), SC nuclei (yellow dashed line),
618 neighboring SC nuclei (white dashed line). Bar: 10μm. **(E and F)** smFISH against *kl-3*, *kl-5*,
619 and *kl-2* (E) or *kl-3*, *kl-2*, and *Dhc98D* (F) showing a single kl-granule. *kl-3* (blue), *kl-2* (green),
620 *kl-5* (red, E), *Dhc98D* (red, F). Bar: 1μm. **(G)** Table listing the genes focused on in this study,
621 their function and their localization within the axoneme.
622

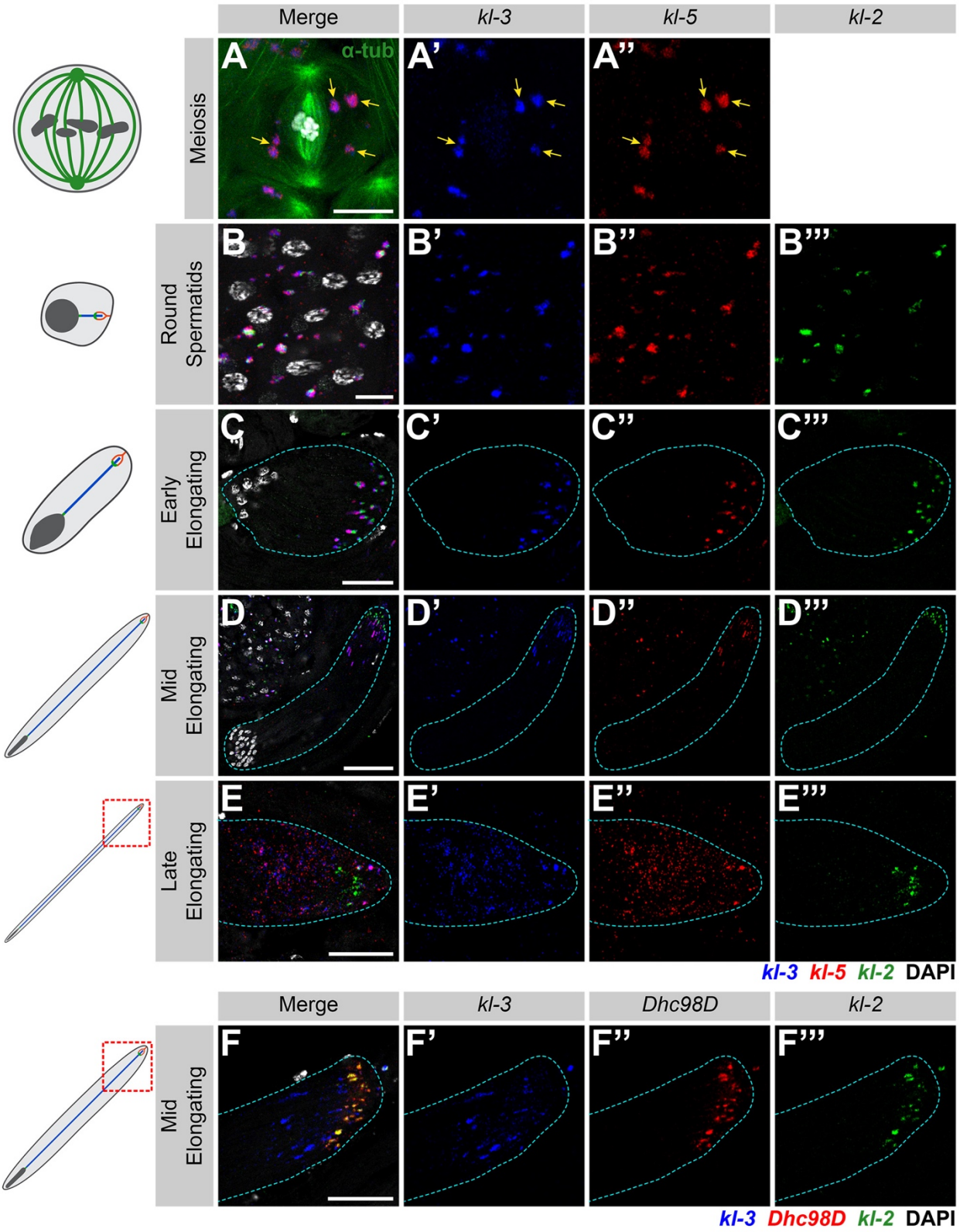

Figure 2: kl-granules segregate during the meiotic divisions and localize to the distal end of elongating spermatids.

626 **(A)** smFISH against *kl-3* and *kl-5* during meiosis. *kl-3* (blue), *kl-5* (red), α-tubulin-GFP
627 (green), DAPI (white) and kl-granules (yellow arrows). Bar: 10μm. **(B – E)** smFISH against
628 *kl-3*, *kl-5*, and *kl-2* during spermiogenesis. The round spermatid (B), early elongating
629 spermatid (C), mid elongating spermatid (D) and late elongating spermatid (E) stages are
630 shown. *kl-3* (blue), *kl-5* (red), *kl-2* (green), DAPI (white), spermatid cyst (cyan dashed line).
631 Bar: 10μm (B), 25μm (C and E) or 50μm (D). **(F)** smFISH against *kl-3*, *Dhc98D*, and *kl-2* in
632 mid elongating spermatids. *kl-3* (blue), *Dhc98D* (red), *kl-2* (green), DAPI (white), spermatid
633 cyst (cyan dashed line). Bar: 25μm.
634

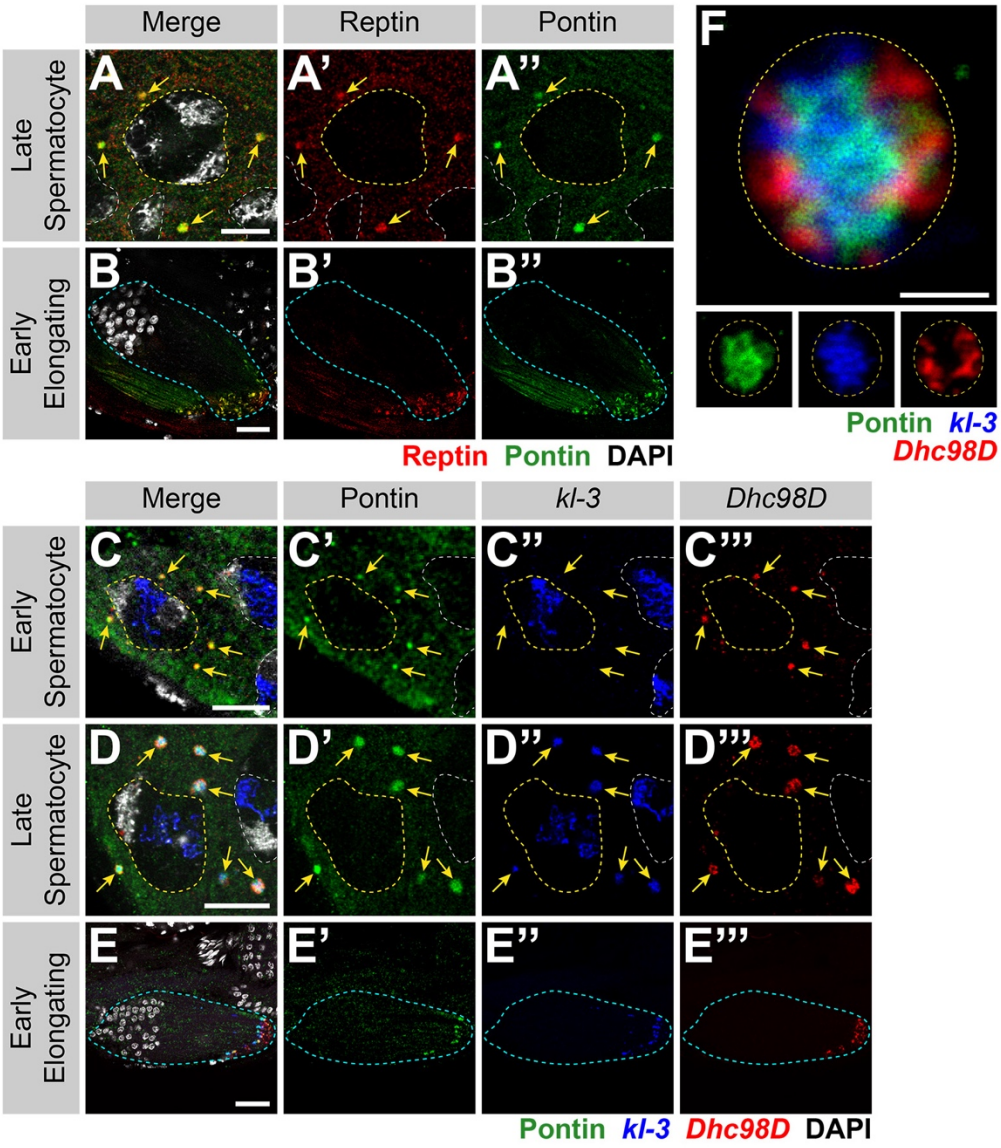

635
636 **Figure 3: Reptin and Pontin colocalize with the kl-granules.**

637 **(A and B)** Rept and Pont colocalization in SCs (A) and early elongating spermatids (B). Rept
638 (red), Pont (green), DAPI (white), SC nuclei (yellow dashed line, A), neighboring SC nuclei
639 (white dashed line, A), kl-granules (yellow arrows, C) spermatid cyst (cyan dashed line, B).
640 Bar: 10μm (A) or 25μm (B). **(C – E)** IF-smFISH for Pont protein and *kl-3* and *Dhc98D* mRNAs
641 in early SCs (C), late SCs (D) and early elongating spermatids (E). Pont (green), *kl-3* (blue),
642 *Dhc98D* (red), DAPI (white), SC nuclei (yellow dashed line, C and D), neighboring SC nuclei
643 (white dashed line, C and D), kl-granules (yellow arrows, C and D) spermatid cyst (cyan
644 dashed line, E). Bar: 10μm (C and D) or 25μm (E). **(F)** IF-smFISH for Pont protein and *kl-3*
645 and *Dhc98D* mRNAs in a single kl-granule. Pont (green), *kl-3* (blue), *Dhc98D* (red) and kl-
646 granule boundary (yellow dashed line). Bar: 1μm.
647

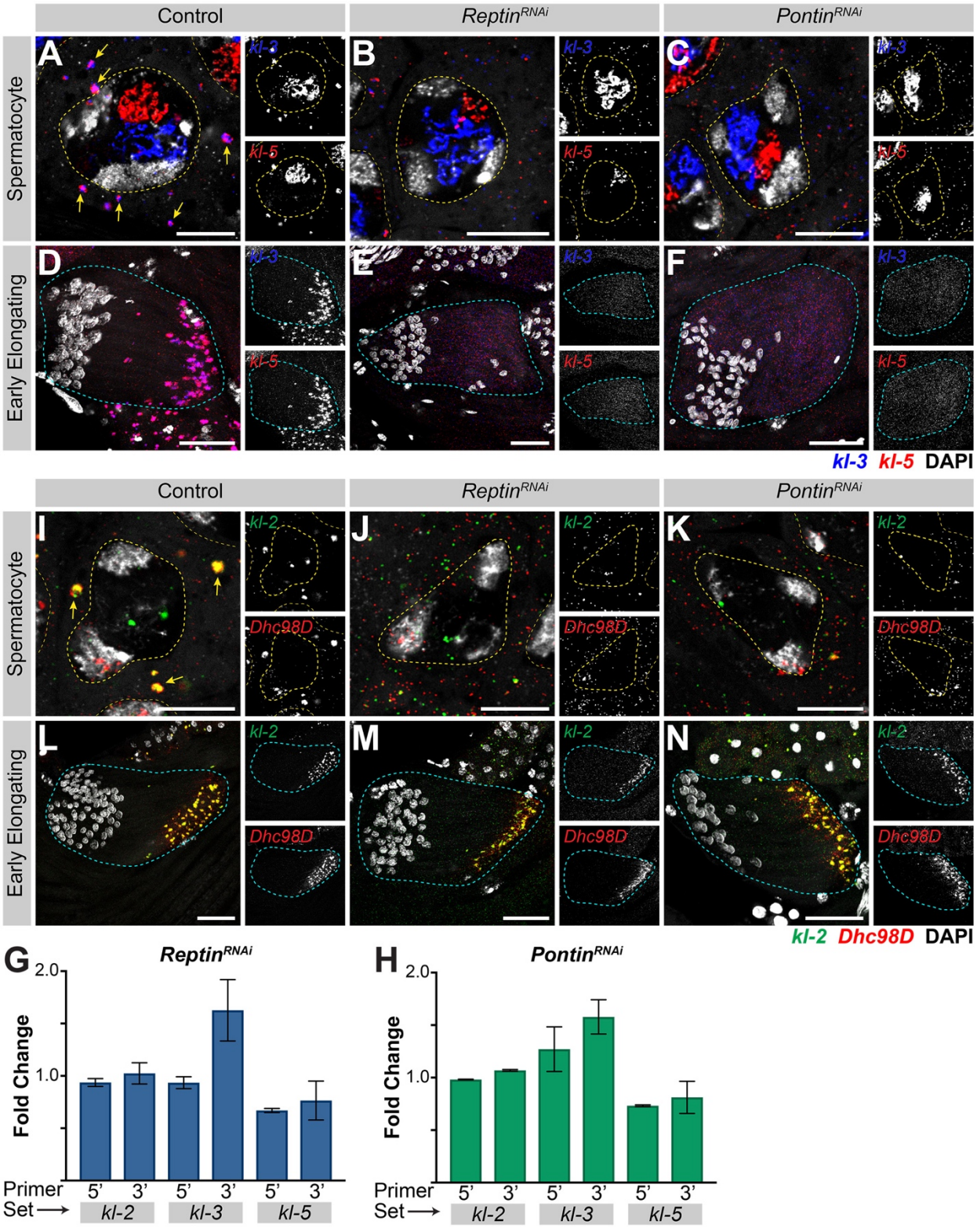

Figure 4: Reptin and Pontin are required for kl-granule assembly.

(A – F) smFISH against *kl-3* and *kl-5* in control (A and D), *rept* RNAi (*bam-gal4>UAS-rept*^{KK105732}, B and E) or *pont* RNAi (*bam-gal4>UAS-pont*^{KK101103}, C and F) SCs (A – C, single z plane) and early elongating spermatids (D – F, z-projection). *kl-3* (blue), *kl-5* (red), DAPI (white), SC nuclei (yellow dashed lines), neighboring SC nuclei (narrow yellow dashed lines), SC kl-granules (yellow arrows) and spermatid cyst (cyan dashed line). Bar: Bar: 10μm (A – C) or 25μm (D – F). **(G and H)** RT-qPCR in *rept* RNAi (*bam-gal4>UAS-rept*^{KK105732}, G) or *pont* RNAi (*bam-gal4>UAS-pont*^{KK101103}, H) for *kl-3*, *kl-5*, and *kl-2* using the indicated primer sets (see Table S1). Data was normalized to GAPDH and sibling controls. **(I – N)** smFISH against *kl-2* and *Dhc98D* in control (I and L), *rept* RNAi (*bam-gal4>UAS-rept*^{KK105732}, J and M) or *pont* RNAi (*bam-gal4>UAS-pont*^{KK101103}, K and N) SCs (I – K, single z plane) and early elongating spermatids (L – N, z-projection). *kl-2* (green), *Dhc98D* (red), DAPI (white), SC nuclei (yellow dashed lines), neighboring SC nuclei (narrow yellow dashed lines), SC kl-granules (yellow arrows) and spermatid cyst (cyan dashed line). Bar: Bar: 10μm (I – K) or 25μm (L – N).

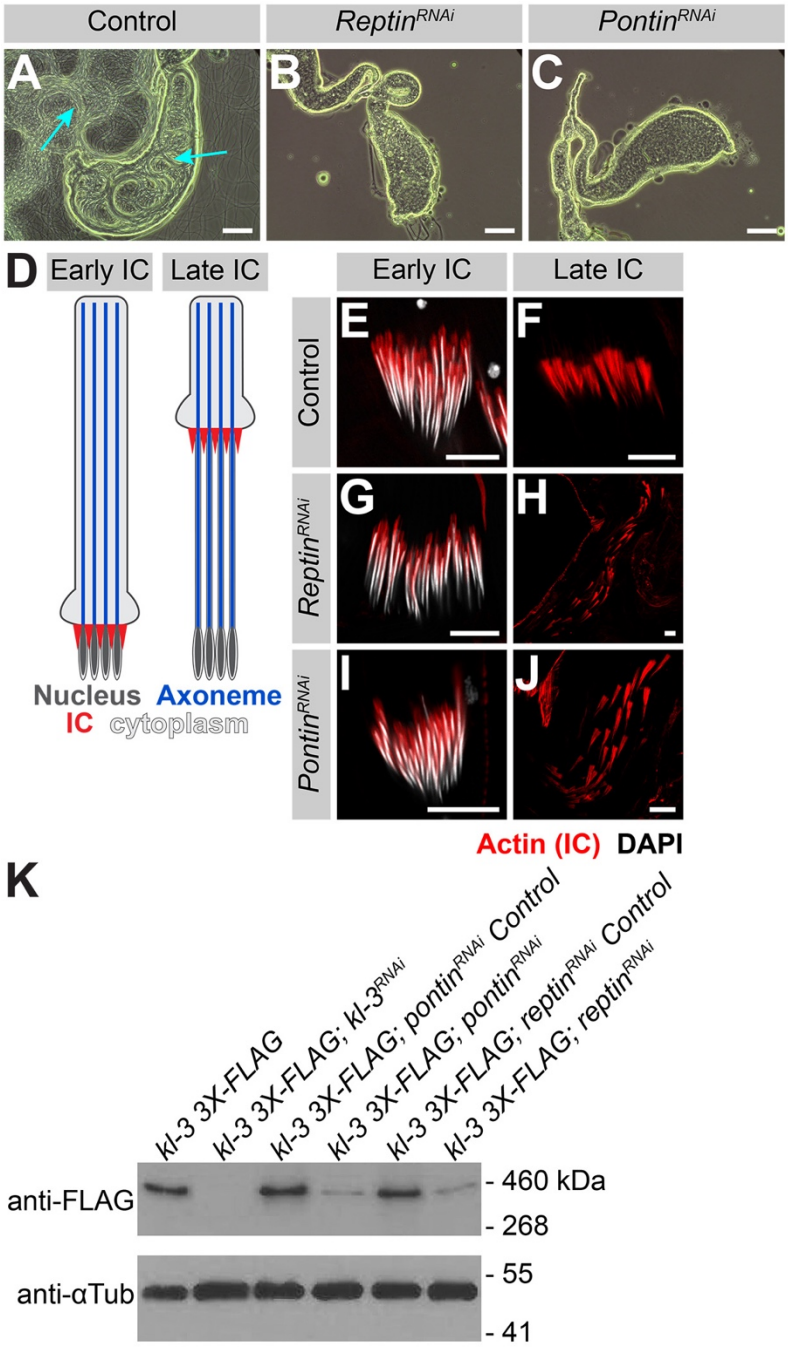

Figure 5: kl-granule assembly is required for efficient Kl-3 translation and sperm motility.

(A – C) Phase contrast images of seminal vesicles in control (A), *rept* RNAi (*bam-gal4>UAS-rept*^{KK105732}, B) and *pont* RNAi (*bam-gal4>UAS-pont*^{KK101103}, C). Mature sperm (cyan arrows). Bar: 100μm. **(D)** Schematic of IC progression during individualization. Nucleus (dark gray), axoneme (blue), ICs (red) and cytoplasm (light gray). **(E – J)** Phalloidin staining of early and

671 late ICs in the indicated genotypes. Phalloidin (Actin, red) and DAPI (white). Bar 10μm. **(K)**
672 Western blot for Kl-3-3X FLAG in the indicated genotypes.
673

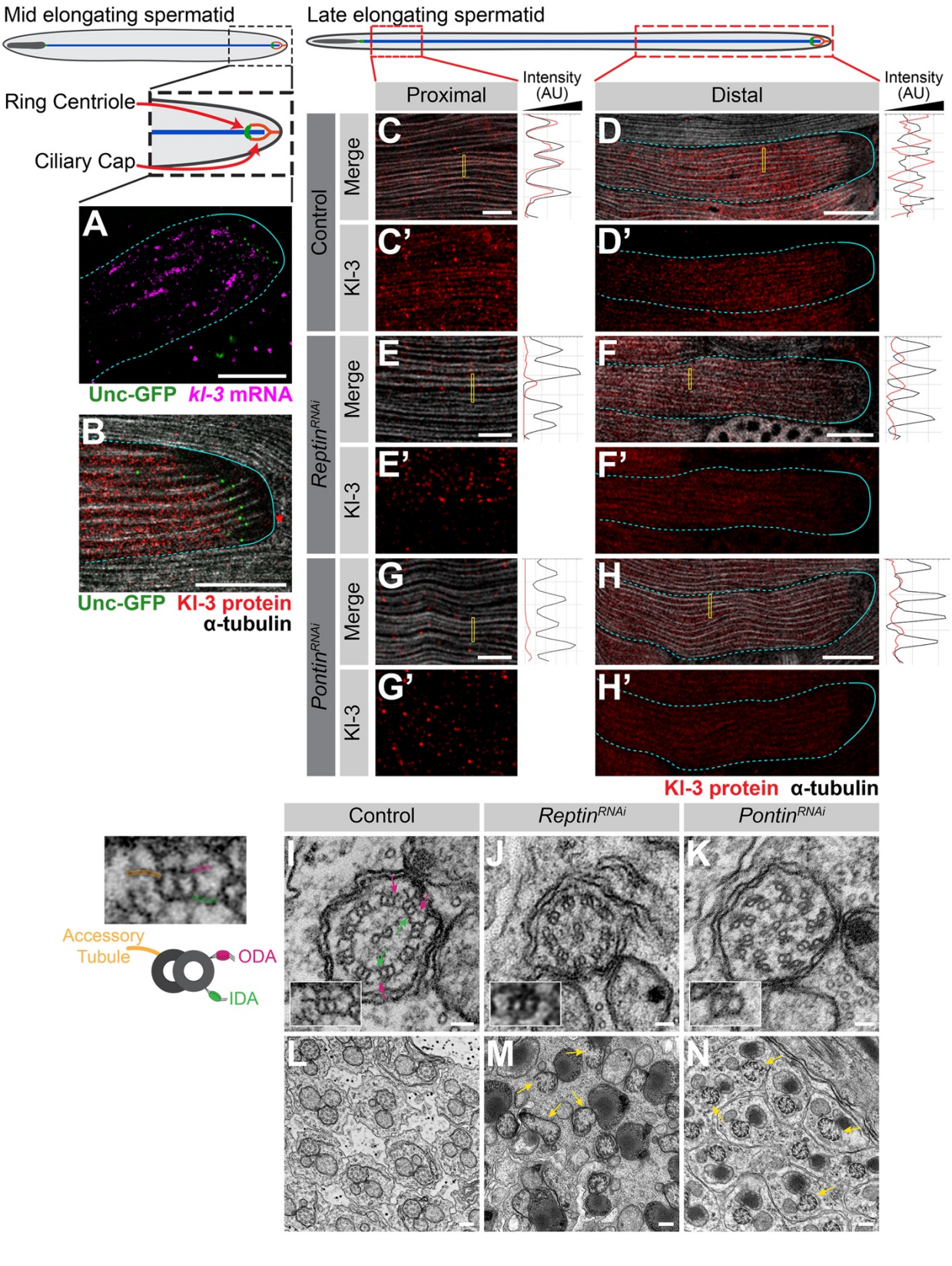

674

675 **Figure 6: kl-granule formation and localization are required for cytoplasmic cilia**
676 **maturation.**
677 **(A)** smFISH against *kl-3* in flies expressing Unc-GFP. *kl-3* (magenta), Unc-GFP (ring centriole,
678 green), transition zone (yellow arrows), and spermatid cyst (cyan, dashed line: cytoplasmic
679 region, solid line: compartmentalized region). Bar: 20μm. **(B)** Kl-3-3X FLAG protein in flies
680 expressing Unc-GFP. Kl-3 (red), Unc-GFP (ring centriole, green), α-tubulin (white), transition
681 zone (yellow arrows), and spermatid cyst (cyan, dashed line: cytoplasmic region, solid line:
682 compartmentalized region). Bar: 20μm. **(C – H)** Kl-3-3X FLAG protein expression in control
683 (C and D), *rept* RNAi (*bam-gal4>UAS-rept*^{KK105732}, E and F) and *pont* RNAi (*bam-gal4>UAS-*
684 *pont*^{KK101103}, G and H) proximal (C, E and G) and distal (D, F and H) regions of late elongating
685 spermatids. Kl-3 (red), α-tubulin-GFP (white), transition zone (yellow arrows), and
686 spermatid cyst (cyan, dashed line: cytoplasmic region, solid line: compartmentalized region).
687 Intensity plots are shown for the regions within the yellow rectangles. Bar: 5μm (C, E and G)
688 or 25μm (D, F and H). **(I – N)** TEM images of control (I and L), *rept* RNAi (*bam-gal4>UAS-*
689 *rept*^{KK105732}, J and M) and *pont* RNAi (*bam-gal4>UAS-pont*^{KK101103}, K and N) axonemes. Pink
690 arrows: ODA, green arrows: IDA, yellow arrows: broken axonemes broken axonemes. The
691 control single doublet enlarged image is duplicated to the left of the figure and colored to
692 match the diagram. Bar: 50nm (I – K) or 200nm (L – N).
693

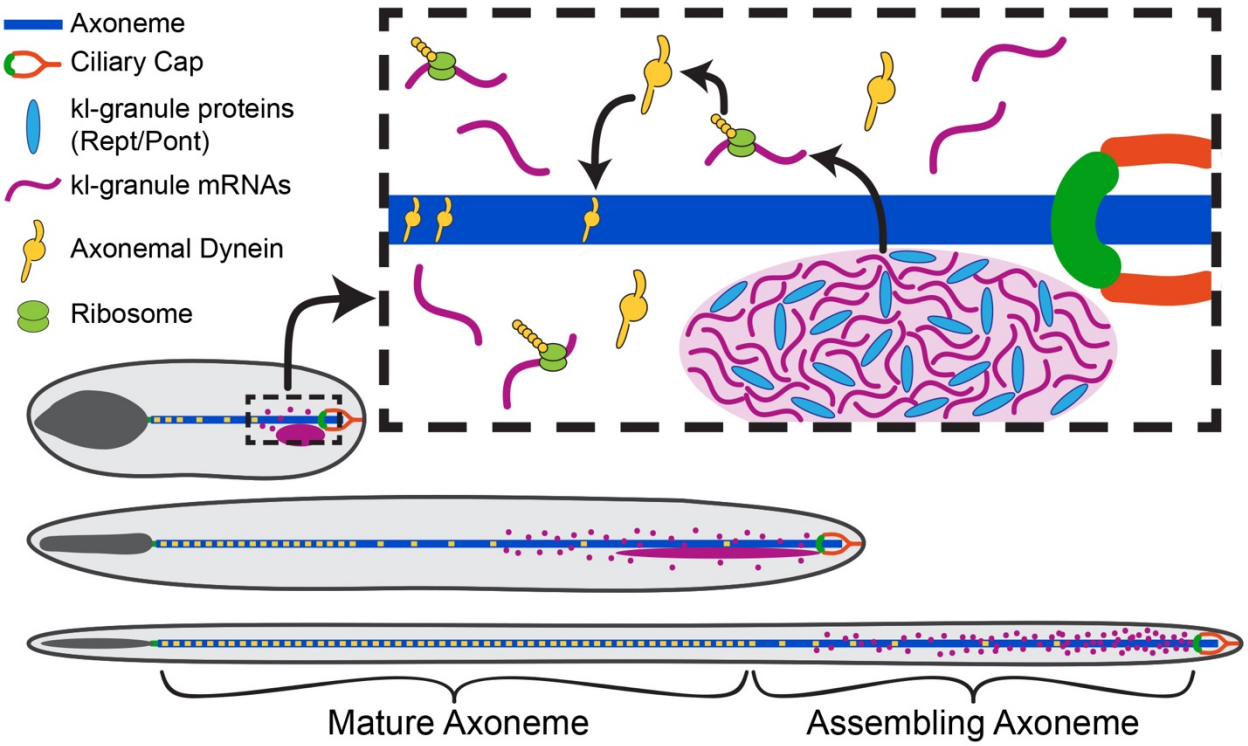

694

695 **Figure 7: Model for cytoplasmic cilia maturation.**

696 The kl-granule (light purple) localizes immediately proximal to the ciliary cap (orange) and
697 ring centriole (green) within the cytoplasmic compartment. Constituent mRNAs (purple) are
698 locally translated (ribosomes, lime green) and their proteins (axonemal dyneins, yellow) are
699 incorporated into the axoneme (blue) as the microtubules are displaced from the ciliary cap.
700 In this way, cytoplasmic cilia maturation is progressive with axonemal proteins being added
701 to the bare microtubules as elongation proceeds.

702

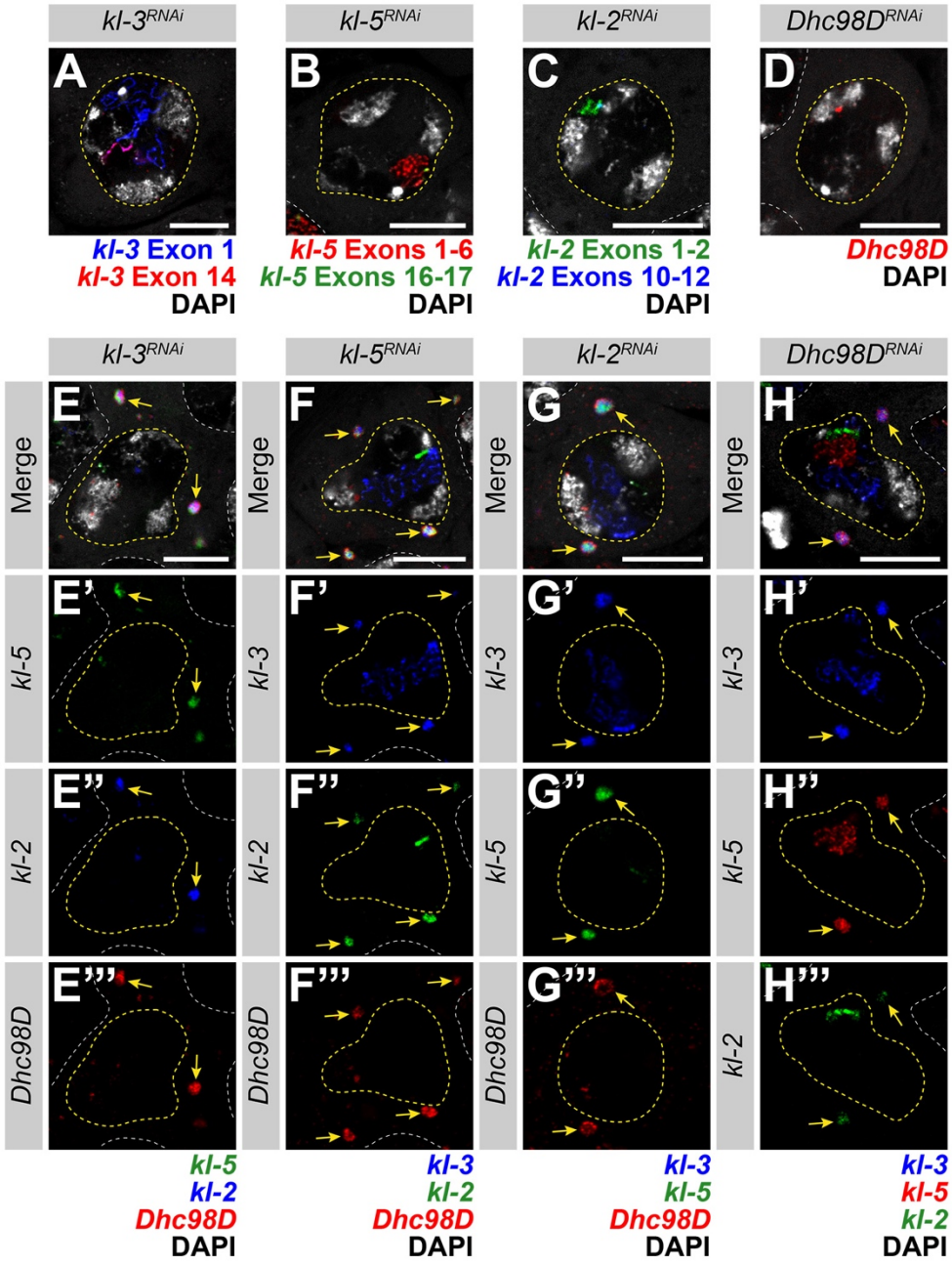

Figure S1: kl-granule formation is not dependent upon any one mRNA constituent.

(A – D) smFISH against each known kl-granule mRNA constituent following RNAi of that constituent shows successful knockdown (no remaining cytoplasmic signal). Note that we use multiple smFISH probe sets for some mRNAs targeted against different regions of the transcript (see Table S1). (A) *kl-3* exon 1 (blue), *kl-3* exon 14 (red) and DAPI (white). (B) *kl-5* exons 1-6 (red), *kl-5* exons 16-17 (green) and DAPI (white). (C) *kl-2* exons 1-2 (green), *kl-2* exons 10-12 (blue) and DAPI (white). (D) *Dhc98D* (red) and DAPI (white). For all, SC nuclei

711 (yellow dashed line) and neighboring SC nuclei (white dashed line). Bar: 10μm. **(E – H)**
712 smFISH against the other three constituent mRNAs after RNAi of the fourth mRNA. Note that
713 the color used to represent each smFISH probe corresponds to the probe sets in A – D. (E)
714 *kl-5* (green), *kl-2* (blue), *Dhc98D* (red) and DAPI (white). (F) *kl-3* (blue), *kl-5* (green), *Dhc98D*
715 (red) and DAPI (white). (G) *kl-3* (blue), *kl-5* (green), *Dhc98D* (red) and DAPI (white). (H) *kl-*
716 *3* (blue), *kl-5* (red), *kl-2* (green) and DAPI (white). For all, SC nuclei (yellow dashed line),
717 neighboring SC nuclei (white dashed line), and kl-granules (yellow arrows). Bar: 10μm.
718

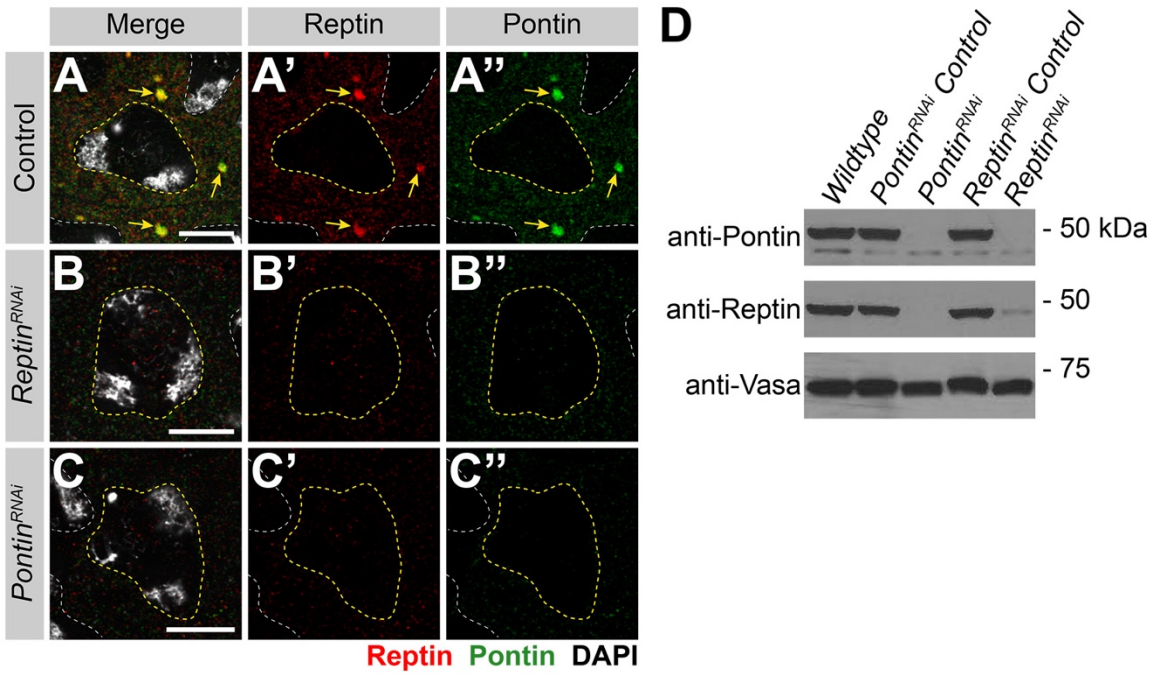

719
720 **Figure S2: RNAi of *rept* or *pont* results in loss of both proteins.**
721 **(A – C)** Rept and Pont protein expression in SCs in control (A), *rept* RNAi (*bam-gal4>UAS-*
722 *rept*^{KK105732}, B) or *pont* RNAi (*bam-gal4>UAS-pont*^{KK101103}, C). Rept (red), Pont (green), DAPI
723 (white), SC nuclei (yellow dashed line), neighboring SC nuclei (white dashed line), kl-
724 granules (yellow arrow). Bar: 10μm. **(D)** Western blot for Pont and Rept in the indicated
725 genotypes.
726

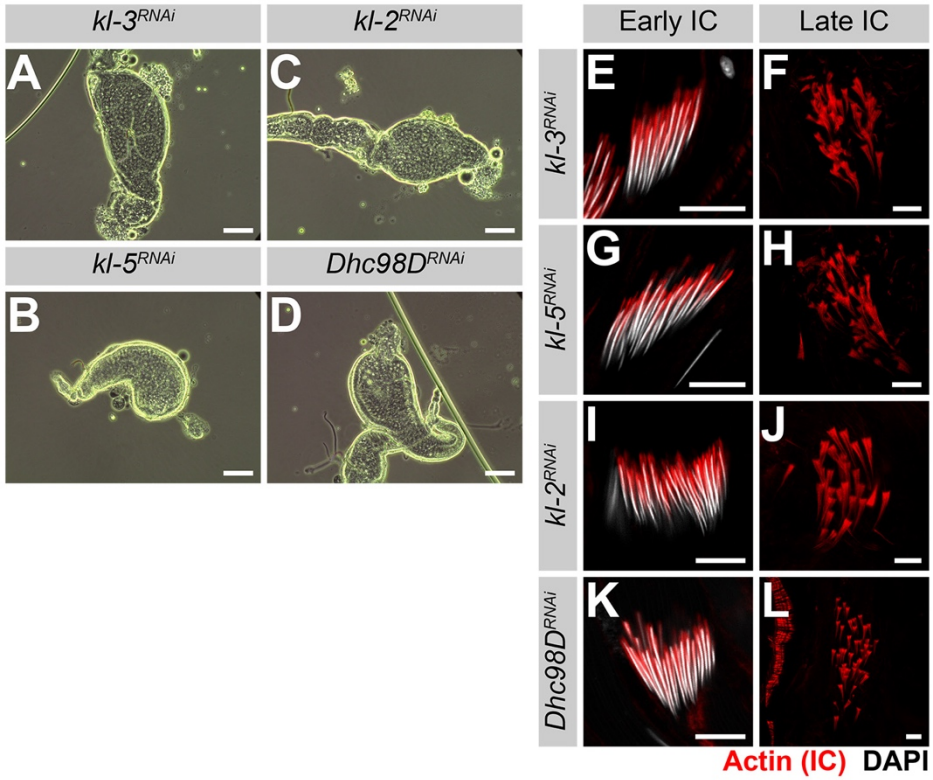

Figure S3: RNAi of *kl-3*, *kl-5*, *kl-2* or *Dhc98D* results in the same sterility phenotype seen in *rept* or *pont* RNAi testes.

(A – D) Phase contrast images of seminal vesicles in *kl-3* RNAi (*bam-gal4>UAS-kl-3*$^{TRiP.HMC03546}$, A), *kl-5* RNAi (*bam-gal4>UAS-kl-5*$^{TRiP.HMC03747}$, B), *kl-2* RNAi (*bam-gal4>UAS-kl-2*^{GC8807}, C) and *Dhc98D* RNAi (*bam-gal4>UAS-Dhc98D*$^{TRiP.HMC06494}$, D). Bar: 100μm. **(E – L)** Phalloidin staining of early and late ICs in the indicated genotypes. Phalloidin (Actin, red) and DAPI (white). Bar 10μm.

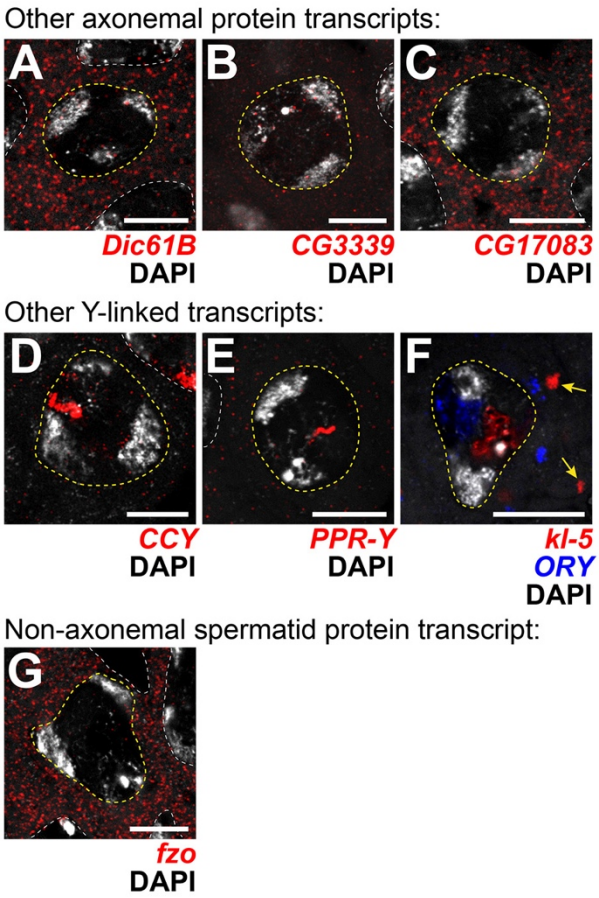

Figure S4: Transcripts for other axonemal, Y-linked, and spermatid proteins don't localize to kl-granules.

(A – G) smFISH against other axonemal (A – C), Y-linked (D – F) or spermatid-essential (G) transcripts. (A) *Dic61B* (dynein intermediate chain, red) and DAPI (white). (B) *CG3339* (axonemal dynein heavy chain, red) and DAPI (white). (C) *CG17083* (ODA docking complex, red) and DAPI (white). (D) *CCY* (red) and DAPI (white). (E) *PPR-Y* (red) and DAPI (white). (F) *kl-5* (red), *ORY* (blue) DAPI (white) and kl-granules (yellow arrow). (G) *fzo* (red) and DAPI (white). For all, SC nuclei (yellow dashed line) and neighboring SC nuclei (white dashed line). Bar: 10μm.

751 **Table S1: smFISH probes and RT-qPCR primers used in this study**

Probe Target	Fluorophore	5'-Sequence-3'
CG17083, All exons	Quasar® 670	aacttcttgatttcctccat, tttccaggaaggcaagcttg, aattccttgtgcttcagcag, ctggacaggatcttcttgta, caaagctggcctcgatgatg, gcgattgttctgttttttgt, tcgacatggcagcgaatcag, tcagagagttaatgtcctgc, ccttctccatgttggaaatc, tatttgcttggacatgcgac, gctgatccggaatggttaaa, cgcattacataggcctgatg, ctccaaaatggtcatccttt, gtaaaaccgcactcctgacg, ataagctgctctcgcagatc, gaaggtgcgatgattcagga, gcaccattttggtgtatgaa, tacttttctcgctgttcag, gagcgtattcgatcagatct, aatgcagccatcgaaggtat, ccttttggccaacaaatcaa, atctccacacgtctcatatc, tgccacctttcgcataatac, caggaaggcggtgttatcac, ctcgaggcttagacttgcaa, tgatcttttgttgtgcacc, tggagaatcttctgcagcac, ccatattgctagattccgta, gctgaaacttatcgatcacc, cgagtaatagagactctcct, catttcgttggcatagttga, attcagcatagttatgtggt, caaacaggcgattcaccgaa, gtgttggagttatccttttt, ggaaatctgatccagttggt, tgttggattcctgtttgtta, agattctccaaacgtgcatc, tctatggaacacatctcgca, tcaccaaggagtttggtcag, taaccagattgacgtgggtg, cgagcagcttcaagaatcga, cgctccatcacataaacact, tgaccacatagtcgaagcgg, tcgcagatcttctcgatctg, gggtgagcacaatgtcattg, atccatgttgaaggcttcac, tgtggacaaggacaccatcg, taaccttctcgtacagcttc
CG3339, Exons 1-19	Quasar® 570	agtcgtgaagctggaagagg, tattgcggcgcacaaagtag, cgctccaagacaatgtcatg, cagtgttatgtactttggct, ccgaattaaatgcggcagtc, tttgggtgcttcgatagtat, gaaaagttccagaaccgcga, cttgtagtccaacattcgtt, agcactttaaactcgccgaa, cattcggctgaagaacaggg, cgcaatcggtggaaagttgt, tgctcaacgagttggcttaa, agagcaaggaattccactgt, ccatgagatccagattttca, tcaagtagattgcgaccgta, agaagttggcaatcagcagg, tggagtacagctgaaactcc, tcctccggaaattcacgaat, cgctggccaaatatttgttg, ttgctgaaggactaacctcg, tccatttttgactgtacgc, acttcgttgtagttctcgat, tgagcggcttgaacacattg, tgcttaacggtactcgagtg, catacatcgtagacttgcgg, tgcaaccgaaggtagacttc, ctggatgtcaagaagtcggg, ttgtcatctagggtttcgat, caatcagagtatcgatgcct, aactgcagcaattgggcaag, agaagcgtggaaaggccaat, gttaccgttggacaagatgt, tttgatgaggtgtcggtcaa, acgaagggcacatactcatc, acgataaacgccggttgatc, ctcctcatttgctggataat, gccgaaataattcgtgcagg, ttcgcaaagcaatcctcatc, actcgtaggcataccgaaac, ggtgatataacagcgatccg, tcctttgtaaatgttgccac, cacgcagatgcgattgaact, caaatcaaggcgaagtccgg, aaatatgggtacatcctccg, aagaggtcaccaatgagacc, ttctcgaactcaaagacccg, gaaaaccgagtgtcgcacat, atccacatgggatcaatgtc
Dhc98D, Exons 10-16 (isoform B, these exons are	Quasar® 570	tcatactggacgaacacgcg, tcgtcaagcatgcgatagac, aacatgtcatagtcgacgct, ttgttgaacaactccagcga, ttgatgctttggtcgatcac, tcatagcattgaccaccaag, cagtaggttctcatgtttgg, gcgtttatctcggtcacaaa, gtcttgagctttttacctag, aagagctgcgctttaggaag,

common to all three isoforms)		ctcgaagagcacctttcaa,	tacgtggcgttctgtatgaa,
		tgtagattccttgcatatgc,	gtcatttgcaattcaggtcg,
		ctgtaggcactaaacgcttc,	ttcttttgtgatgtgtcacc,
		ttactgaccatccacatgat,	ataaacgctgtgcattcctg,
		acatctttgggcttcttatc,	cagcagatattgggactctg,
		aagacatcgcgcttcagatt,	actgctgagcttcaaacagg,
		gactgcgggaagtgtaaagc,	gcaggtccttttcataatc,
		ttgacctatacctgtcaacg,	gtaggaagatcacctctgac,
		cacgcccatttggataaaga,	tatcgatacgagagcgcaga,
		gtagatacgattcgccagag,	gacatggatatatgccggat,
		ggagtcgtaaagcttcttca,	ttccagaaaatgtgcccaac,
		tacacttgaatgtctctcct,	ggcggttgatatagcatttt,
		gacatcaggagaacagcgtt,	tgaaccgaaggctcaaggac,
		ggtcatccaacgggtgaaaa,	ggattacgtcctcatagtac,
		tgaccagatccacaatggat,	ccactctagaagccaaatcg,
		tgaaactcttctcgaaggcc,	ctcatcgatttcgatgagcg,
		gtttccacaatggacgagta,	cacacttgatgtcctggaac,
		cagcaagggctccaaattta,	cctcatgttatcgttgacat,
		gtggtcttgttcagattcag,	atttcgtggattttctgctc
Dic61B, Exon 4 (isoform A, common with other isoform)	Quasar® 670	gttcccagttaatagtttca,	cttcgagagcctcaacagtg,
		aaggacttggtatacggctt,	gacttgcgtaaggtgatctt,
		gtctggctgtgaatttcgaa,	cagatactcgtagtttcggt,
		aattttgcctttccctattg,	tctgagcgtcattgtctgag,
		gagtggtgaagagcagagta,	ggttatgaggatggtgttga,
		aacgtaagagctgacggtgg,	gcgtgtcgtacatctcaaag,
		actccttggtgatattgttc,	cgaactcatagtggctgttg,
		tcgtcgtcctcaaaggtatc,	cttgtctttttcggcaacgg,
		cggaacaggcgctctatctg,	atgatggcgttgcgaaactc,
		tcgtttgtgttgctcgagag,	ggtcaaagttacggaagcgt,
		catcgagtagacgtactcgg,	taccagccgaaagagcaagt,
		cggcagaaatcaatgtcgct,	tgagtacagtccgtaggcta,
		cggtacgtgctgtgaggaaa,	acaggaaaacgctgccggag,
		ctcgcctggatttttaatgc,	acatcgtagtagtatgcgcg,
		aagtttattgccgttactgg,	aaggatggcaagaatggcga,
		tcgtacagaccaatggcgag,	tgcaaactgctcacatctcg,
		aaacttgtttgatccagcgg,	tgtctgtttcatgatcgtcg,
		gagaggctcaggaatggatc,	tgataatccggaagcgggtg,
		aaccaagcaggaagggactt,	actcgctccagaatcatttg,
		gaacgaaaatgccctcagga,	ttagactcgcaggggatacg,
		gtagtgatgcttaagccttg,	atgtccttgtgcagaggatg,
		tcatctgtcagcacgtagta,	gattgagcacttgtggatgc,
		ccaagtactgatgctgataa,	cgtcgtgacaacgcaggact,
		gaactccattacggtgacac,	aggtgaggaagagtttggga
fzo, All exons	Quasar® 570	aaacgaggacaccgacgacg,	gcgaagacgacgatgaggat,
		gcgtccacaaactcacttaa,	tatatatcctgcagttctgt,
		tttaacaggacagtctcctc,	aaagaacctttgcaatggcc,
		gtccaaaaaatgccaccttc,	cattgatcacggcacttttt,
		gcaggatttttcatgcaga,	aaaacagctggtggtatggc,
		cagagttgagggttttaggg,	atccaatatcgagcaacggt,
		tagctatctaggcaatcgtc,	actcggcgttgagaactaga,
		ttgaagaactgcctttccac,	agagatttggacgcgagagt,
		cccatcgattgttgagtata,	caacgttccatatgctgatc,
		acacctaattcatccacgag,	aacatgatagatcctttccc,
		cgtaatctgaccattcctta,	gaaactcctgatatcgctgt,
		accgcgaggcaattcgaaaa,	acttagcaagtgtggaccaa,
		ctctatttcggcattcaagt,	tctatcctcttgcattagta,
		gtcatttcagtcagttcttc,	tctggtcgttcaaaacgcac,

		gatagcacagacgagggtat,	ctgggaattccgggtgaaat,
		ataacgagcgttggtactgg,	ggggtatggagagacattga,
		aagcccaatttctttctcta,	tagattagttgccaatcgca,
		tctggctgaaagtcactcat,	ttcgaaatggacttgcgtgc,
		tccgttaactaaaggtggca,	ttcaccaaagattccagcat,
		tcagtaaaacggtgcccaag,	ccagttgaacgaacggatgg,
		cccaccaaggatcaatacaa,	cttgaaacttcgctcttggg,
		ctaacagtttgctgcacatc,	gtcgcaactggagctcaaaa,
		attcagtgtctcattggact,	tgtatttgtttggtcagctc,
		gaaacttcttcaggctgagc,	taggtctcttgaaagtctcc
kl-2, Exons 1 & 2	Fluorescein	Cgatcagtctcagtactttc,	ttcacatattcaacaagccc,
		tctgttgaattgatcaacca,	gtgagaacatcgcaatcgta,
		acaggaaatccaaggcaacc,	cataaatcaataaccggggc,
		ttatttctttagaggaccga,	cgaagttaaccatgtcgtga,
		caacatcatcttgcacagta,	aaattttcaataggcagcca,
		tgggagcatatataagctct,	cccattccataaaatttcga,
		aacgttgcttcacattgtct,	atttatccagggacgtacag,
		ttgctgttaagattcctaga,	aactgtcatgccagacattt,
		ctcttttgctatttctttga,	attctctgtcgtacgatgaa,
		cgcaatacactccaagttct,	aattcgaataagcgtagccc,
		tggtaagggtcttgtcattt,	ctcatccccaacactaatat,
		accgatatagccagaactcg,	tgcgcatttagtccttgaag,
		ttgaacatccacttgatcca,	gggtacttcgtagaactctt,
		attagttcatcgatctgttt,	ccatcagttcatgtgtagat,
		atttgatgttttccatagct,	gttgtgaacatggttgcatt,
		gtgagacaaaagttgggctt,	tcaagtgaattgttcgggga,
		gtattgttcagagtttaacc,	ccagttattaaatcacgtct,
		ccttttcagtacaaaaccgt,	tccaaaccttgaacttcctg,
		attcctttataagtcaggca,	ttttgcatgggtttttgaca,
		ccaacctattcgtatgttta,	aatcattgcattgtcaaggc,
		ctccataaaggcatcgacat,	gtcttccgaaaaccatcatt,
		gtatactctctgattcgtca,	taccaccgaattgaggctta,
		gcttcaaattctgtaccact,	attttcaacgttgtcggcag,
		ataatgccgtaagagtcacc,	atgatctctttggaatccgt
kl-2, Exons 10-12	Quasar® 670	tcgttcgagtaggactgtat,	cattccagccaagttctaaa,
		ggagtgtcttcatattcatt,	agatactttaaagctcccca,
		ccgtaatttactcctgctat,	caatcgtcggtaatgtgtcc,
		gttattaatagtcggcgatc,	tgcaatgcttggtcacagaa,
		aatatgattgcacatcgccg,	gggaaacatttgtatttggt,
		gtccaaaagcatcaggctta,	tgacgctatatcggcatttg,
		aagcattcttgtttctccta,	ttgcatagaaagcagagcct,
		acttgtgctattagtctgga,	ttgtctcaccgttttcatta,
		tttatctcatccggtgtatt,	aatttttgccgtctgttcat,
		gggagttcgattgattccaa,	agcgctcaatttcttgaagt,
		gagtggacatgtcaacgaga,	ccacgtcttaagtcacgtaa,
		attacaacaagtccctgtat,	atatcctctaagtccgaact,
		ccttcagagacagctagata,	ttaaccattgtaatggcacc,
		tgccgctaatggtttcaatg,	atgtattaagtctctagccc,
		gcccaactattaaaatgtcc,	taatattggagggcggagtg,
		cgtgtaagctgcaagccaaa,	gctgtaacaaatccagttgg,
		ctcgagctgaagtttgtagt,	tcccaagagagttcatcaat,
		ggcagtatcttcttcaacaa,	ttcccttattatacgagctg,
		tcgaatgtaaacgcctcctc,	gccaccctccaaaaacaaac,
		attggtttttcctcaaccat,	atcggtagtggatcctgaag,
		gtgtattactggtaatggac,	taggttttctactggcttaa,
		aacaccacgacatcgttttt,	ataatatgcgggacactggt,

		aatgatcctgacctaacggg,	ctttaagtccacggctatta,
		agtagtcagccttttcatta,	taaaagtgcagtacctcgct
kl-3, Exon 1	Quasar® 670	taacattccttctggatcc,	cgcgaaacgccaaagagttt,
		gcagcacgctttaacatgtt,	ttggtcacttacactaggtc,
		tatcgtcttctttgttggtc,	cctcatttctcgaagtaact,
		caggcttgaaatccgttgtt,	aaacataccgctggtttggg,
		atacccaacaaatctgcaca,	gttactatttcctcaggatc,
		ttgctttcatccacaatacc,	accatttacattctcaacat,
		gggacctttttcctcaaata,	cgttacttatcattatggcc,
		cggaatcagttggatatcct,	tttaagcttttcctggtagc,
		agagcgttgaatttcagtgt,	actagatccgacctcaaaca,
		gtcgatatacaacagtccac,	accgaacggttatcaatcga,
		aaatattgccacctcatcac,	aagcaagagtttcgctcttc,
		cggctttaaaacgtgatcca,	caaattcggtcacagcttct,
		tgagtttgctctttttctgc,	acagttgcttcagatgattt,
		cctttaaatagttcatgcga,	tttgccatctcacaagtaat,
		gtatttttgaactggcttca,	caaccagtcgaactcgtgta,
		gccattgctcaaaataacgt,	gtataccttgaatttgtcga,
		gtatttgttttccctctact,	ctacatcgggtgtatctctt,
		ccaattgaccaacatttgca,	tatatctggccaacatacgc,
		gtaacaaactccgttatggt,	gtggttattaaatgctcggg,
		agataatgtcaagcaatcct	
kl-3, Exon 14	Quasar® 570	gtactttgacatagccatgg,	aagatttgcctttaagggca,
		tgatatttagcctcttgcac,	ctgcttcttgtagatcactt,
		cgttttctttttgttgcagt,	tttttggcctcgtctaatac,
		aaccaccaataagagcggtt,	ttcagtccatcggatttttt,
		cggtcggtctcacttttaaa,	ggagaataacatctccgacc,
		tcttgattaaatggtcccgt,	atgttccactcaccaatttg,
		ttgacagttcatctgttggt,	ttttaatccacacttttccc,
		taatcggaattcccatgcta,	taactcctctgcaacatctt,
		aaggttgtccaagcaaggat,	tccaatccacttctttatca,
		gattgggtagctttgttgta,	cgcgcaaatatttcaggtgt,
		ccacgcattgtcacagtaaa,	gaacccgttcatcttctaat,
		tttcatgtttccagtcacag,	ttcctttcgtagtggacaac,
		cctcaatcactgtaacgtcg,	tccttaacttcaatggcagt,
		cagcgtttatttttgcttct,	acactacctcttgtagcaac,
		gcatcaaagcgctcaaggaa,	tcctctagatttgtagcgat,
		ttaactcaagctggcgatca,	cgcaccgccttttataaata,
		caccgaaacggaacaggagg,	tataccacgtaaaccaagcc,
		ccatacaccacgaacgaaca,	agtttagtactactggctcg,
		aatcattggcataagttccc,	agctcatttttttggcgag,
		cttggcccatagaaatagga,	cgtcttctaggcaggataat,
		tcctaagtgacagttttgca,	actgtaagctctaccatgta,
		agcaggtggttcattagtat,	tttttagtccagcacgtatt,
		tggagattgcgaatagtcca,	tgcataccagtcggatgaat,
		tcctgctccttaaaactgta,	cgtttgccatgtcatcaata
kl-5, Exons 1-6	Quasar® 570	cttcttttccttttcgtcag,	aaaaactccggacggttgtc,
		ttgtcttggttaggtagttc,	ccacttatccagcttaagac,
		cctaaactcgttggttgtta,	atacgtttcttgttgggatt,
		ccaccggaattgattgtgaa,	ctggaaagctgtaggatgga,
		agcaactttataccgtggtc,	gaagtggtgttaagtaccga,
		atttgctaatgggttcggta,	atcccacttgatttactgtg,
		tctgtcttcatatcgtttgc,	tccatttcgcatttcttgag,
		aacgagacctttcatctggg,	catgacttcgtccatgcaaa,
		gcttcataagagggttaacc,	caagccactttacaaccata,
		tttacgaggtcttcaacgga,	tgcctctggtagtggaaaat,

		caagttctcaaggttttcca,	agtctttatacgcctatctc,
		tctgcgataagaatgctcga,	acttagttatgtctctagcc,
		gtccatatcgtttgtttcaa,	gtcgtatatctgatcggttc,
		cactaatccaattgtcagca,	tgaaaataccgcgagtgacc,
		gttctgttgacacagtcgat,	ggaatatggagtctggttct,
		ttataggcttcgtcgacatc,	tgtaatactctaggtgctgc,
		cagtcctgcgagttaaatgt,	atcgtccgaatatttcatcc,
		tcttttagctcttccaatcg,	ccccataacaatttttttcca,
		aagggcgaaagttatctgcc,	tgctgttgtactcttcaaga,
		aatatttgtccactcacggt,	acagagaattttctgcgtcc,
		tggccttgaagcttaaacga,	tgaaacgataccatgcgctc,
		atgtgtgtcttcaagacctt,	gcgaagaagtaaggagcctg,
		gggttcgacatgtttttga,	atcatccacaatgacatgca,
		taacgcacatgatctcttcc,	cgagcgccgtaaaaacgttt
kl-5, Exons 16-17	Fluorescein	ttgtggtccgaatttcctac,	taaacgggtagctacggttc,
		tgatattgtcaaatcgccca,	ccaggtaattgtacagcaca,
		caaggtactctggtattggc,	ccatacataatctctccgaa,
		ccagtcgtctgtaatgtgac,	gataagttcggcataagcgg,
		agctctggctgcataaattc,	aaaccctggcaatactctag,
		atttaagtattcctggagcc,	atgtaattgtggtagccagt,
		gagatggactttcagacgga,	gcatttgaatgaaggccgta,
		cgtagttaggaacccaatct,	attcggaagagtcgttcaga,
		tctcggctgcaactcgaaaa,	aaactgtctcaccaccacta,
		gtttttataatgtcttcct,	aatggtgtgggagttttgtc,
		cgcgacccattagttctaaa,	atgtatggacttcggtcttc,
		cgctcacactcttgaaatgc,	gcttcaattcagtcataaga,
		aggtcaagctcattcagaga,	agtcaattctcctttaaggc,
		ccattaaatcctccataact,	gcacttggtccatgtaaaga,
		aaccaggattgtagccctag,	cagccgcaacattaaatcgg,
		aggcatgcgaaagtcggcaa,	atcctgccaaccaaattgat,
		aggagcgactgaggattaaa,	cgtctgttgcatgatagctg,
		gacacattctatcgagaggc,	ttccacttttggtgacatc,
		ttgatataggcaccctctcg,	tgctccctccatgaaaagac,
		aatggttcccattttcatgt,	gttcctttaaaaaggcgtct,
		agaacaggcatagcaggaaa,	cttgggttactgcctttatg,
		gacatttttaatatcctgct,	cggattttgtaaactgggca,
		caaacgaaggtgggtcctcg,	ctctcggcttttcaagttaa,
		ctagagtccacttacttgct,	tgcaagagaagacaaacccc
ks-1 (ORY), All exons	Quasar® 670	tttttggctttctttctgtc,	aaaagttgaggctccgagtt,
		cgtttaattcgcgatgcttc,	cttcatctacataccgacga,
		tccgatgttgaagtcagttc,	cccccaacaaatctttaagt,
		tgatgcatctgattctttcc,	tcttgcactaactgttctcg,
		cagttgtaccactatttcgg,	ttagctcgagaagccatttt,
		attcaacgtttaggcgttcg,	ccattgtcttcatcaaagct,
		tttccatgtgcttctttttg,	ctctattcgcaatatccagt,
		agtttacgtgtcgtttctga,	gcattgccttatttaatgcg,
		gccttaactgctttatcatt,	aagcctgctcgttaattgag,
		ttgtacattcttgttgtcgc,	catccttctccagagaatta,
		gacgaatatcatccgttcgg,	cacgttgcaatgtctctttg,
		atgttttaagtccgccatag,	tctttctctgctttggattt,
		cgtcttcagagagatttggt,	tcgtgtaacttttccgtgag,
		acggactccaactgtttttt,	cgctgaagcatcattttctc,
		ttttacttcgtttgcgctta,	gccactaagttttctttgtt,
		tttctctcatatccttacgt,	caatccgactaggttacgtt,
		aacaatctcgtcattccgtc,	gggcattttgtgcaatttga,
		aaggcattcactttcagtgt,	ctcatgtcagcagtactttt,
		tcttcagttagagctcgtat,	caacgatgtactcctgtagg,

		aatttcttaggatcttcgcc, tattgactgctttagggagc, agcctcacacagtttatttt, gcatatgagatagcatcctt, taatgaacgctctgctgcta, gtcttgatttaagttccacc, aattgacagctctccgattt, tatttcgtttttcccatctg, atccacattccatatactct, atatccgttaacttcgcaca
ks-2 (*CCY*), Exon 1	Quasar® 570	tcttttgtgtggagaacgc, gttaagctcataactttcgt, attaacgcaaactccagtgc, cgatcgtcgattgaagatgg, ttcttcgttttctgaccatg, tcggcaacaaaacgcgattt, tggattgttacatgccacta, ttcgtttccatgctttacaa, cagcaggagattactaccat, ccgcatttattaagctgtct, gtaaccaatcgattgcgtca, gctggttgttaaggatgttt, agcttcatgtctgattcagg, cgcgttatccatttttatcg, gcgttgatttataatcctct, cctagcattatctcgattgt, ccatttagctttacttgcag, tcattctttgagcttatcca, ttcttttagttccttctctt, ccatgtcatcgatagttctt, cctcaagtaaatcctgggtt, gctttaggtaagcattttcc, cggcatcgaatggattgttt, tttgctcgggattaatttct, gaaggtactcaacgtctgtg, gccatttcgttaatttttcg, gccgaagtagcgataattct, cttataagcatatcttcggt, ttctacacatttgtgcgcac, cttgaaagcttcgttgcact, gcattattcatatagacacc, tttcttgtagaattctctgt, acttttacgcagagcatct, caagcgcttccagattttta, tgttctagggcattaagctt, aatgttttctgcctcatttg, attgtcttcaagatcctcag, gtttatgtattggttctgct, atccatttcctgctgaatat, agtttctctaatccttcgc
Ppr-Y, All exons	Quasar® 570	atttatttgatcgtcttccat, aataacttcatccacaagggg, tattccaggttcaatatctgg, agctttcaatcaaggaacggt, caccacgatgaacgtgtttta, cagttgatgtaaacgtcttcc, atttgttccaatacaacaggc, ttaaactccaaacgcattgtt, atccataagtgatcaatacgt, taaggcaaagcttggtcagat, aatggtctctattttgttgca, ggtgtcaagattttcgatctt, gacagaacttccaaatttact, ctcaatagcttcaattttgtt, agcatggttaacatatcgata, tatttccaaggctgataatta, tccttcaactgtgtcaattaa, ttcataaaccgaaatcgttca, gataggattaccttccaaatt, ctgatatgtactttaacaggc, cggagttcactcttaatgaaa, agtataaattacaggcttctg, tcttcaatttcccgaatctcc, cttgtatctccttttcttgtt, tctgattgttcacgttcaaga, aacttgaggctaatcgttttg, tgatgaccatccaaatgttca, cacgccaaagtgagtcaaaca, caacaagcatcagcacacgac, atatccttatcgtattcgtcg, gtaaatttcttgcgtaagttc, gtaaatctttctaagccaagt, tctcgaatttcttcatcgcgc, tatttgaagttcttcttggcc, acataagctccgcaatttttc, atgcttgagattgttctacaa, tcgagtcaatatttcggtcat, gtcttgaagtgcaaatttcgt, tcggagttcaataggaacgtc, ttaaaatggcgtcacggtcat, ctcgctcatctaatcgcaaag, gtctacaaattcctttgttcg, ctgtttagttggtctatcata, aatttttgaccgatgtcgttc, catcggtcatcatttctacaa, cttacatcgtgtggtaaggat, acataatcttcggctatcagc

Primer Name	5'-Sequence-3'
Gapdh-qF	TAAATTCGACTCGACTCACGGT
Gapdh-qR	CTCCACCACATACTCGGCTC
kl-3 _exon1_qF	CCCGAGCATTTAATAACCACAAG
kl-3_exon2_qR	AACGGACATTATCCTTAGCTTCA

kl-3_exon15_qF	GCCACGAGCTCGATGAATA
kl-3_exon16_qR	AGTACCTTCAACGGCAAGAA
kl-5_exon1_qF	ATGCGTCTTAAGCTGGATAAGT
kl-5_exon2_qR	TGTCCACCGGAATTGATTGT
kl-5_exon16_qF	GCCTCTCGATAGAATGTGTCTT
kl-5_exon17_qR	TTTCATGTCCCATCGTGCT
kl-2_exon1_qF	AATGACAAGACCCTTACCAGTC
kl-2_exon2_qR	TTTGTTGAACATCCACTTGATCC
kl-2_exon5_qF	CGTCGGACTTTGCCCTTAAT
kl-2_exon6_qR	GCTCCAAAGTGAAGTTCTTCGAG

References

Anderson, P., and N. Kedersha. 2009. RNA granules: post-transcriptional and epigenetic modulators of gene expression. *Nat Rev Mol Cell Biol*. 10:430-436.

Avidor-Reiss, T., A. Ha, and M.L. Basiri. 2017. Transition Zone Migration: A Mechanism for Cytoplasmic Ciliogenesis and Postaxonemal Centriole Elongation. *Cold Spring Harb Perspect Biol*. 9.

Avidor-Reiss, T., and M.R. Leroux. 2015. Shared and Distinct Mechanisms of Compartmentalized and Cytosolic Ciliogenesis. *Curr Biol*. 25:R1143-1150.

Baker, J.D., S. Adhikarakunnathu, and M.J. Kernan. 2004. Mechanosensory-defective, male-sterile unc mutants identify a novel basal body protein required for ciliogenesis in Drosophila. *Development*. 131:3411-3422.

Barckmann, B., X. Chen, S. Kaiser, S. Jayaramaiah-Raja, C. Rathke, C. Dottermusch-Heidel, M.T. Fuller, and R. Renkawitz-Pohl. 2013. Three levels of regulation lead to protamine and Mst77F expression in Drosophila. *Dev Biol*. 377:33-45.

Basiri, M.L., A. Ha, A. Chadha, N.M. Clark, A. Polyanovsky, B. Cook, and T. Avidor-Reiss. 2014. A migrating ciliary gate compartmentalizes the site of axoneme assembly in Drosophila spermatids. *Curr Biol*. 24:2622-2631.

Bley, N., M. Lederer, B. Pfalz, C. Reinke, T. Fuchs, M. Glass, B. Moller, and S. Huttelmaier. 2015. Stress granules are dispensable for mRNA stabilization during cellular stress. *Nucleic Acids Res*. 43:e26.

Boisvert, F.M., S. van Koningsbruggen, J. Navascues, and A.I. Lamond. 2007. The multifunctional nucleolus. *Nat Rev Mol Cell Biol*. 8:574-585.

Breslow, D.K., E.F. Koslover, F. Seydel, A.J. Spakowitz, and M.V. Nachury. 2013. An in vitro assay for entry into cilia reveals unique properties of the soluble diffusion barrier. *J Cell Biol*. 203:129-147.

Briggs, L.J., J.A. Davidge, B. Wickstead, M.L. Ginger, and K. Gull. 2004. More than one way to build a flagellum: comparative genomics of parasitic protozoa. *Curr Biol*. 14:R611-612.

Buchan, J.R. 2014. mRNP granules. Assembly, function, and connections with disease. *RNA Biol*. 11:1019-1030.

784 Carvalho, A.B., B.A. Dobo, M.D. Vibranovski, and A.G. Clark. 2001. Identification of five new
785 genes on the Y chromosome of Drosophila melanogaster. *Proc Natl Acad Sci U S A*.
786 98:13225-13230.
787 Carvalho, A.B., B.P. Lazzaro, and A.G. Clark. 2000. Y chromosomal fertility factors kl-2 and kl-
788 3 of Drosophila melanogaster encode dynein heavy chain polypeptides. *Proc Natl*
789 *Acad Sci U S A*. 97:13239-13244.
790 Caudron, F., and Y. Barral. 2009. Septins and the lateral compartmentalization of eukaryotic
791 membranes. *Dev Cell*. 16:493-506.
792 Chen, D., and D.M. McKearin. 2003. A discrete transcriptional silencer in the bam gene
793 determines asymmetric division of the Drosophila germline stem cell. *Development*.
794 130:1159-1170.
795 Dafinger, C., M.M. Rinschen, L. Borgal, C. Ehrenberg, S.G. Basten, M. Franke, M. Hohne, M.
796 Rauh, H. Gobel, W. Bloch, F.T. Wunderlich, D.J.M. Peters, D. Tasche, T. Mishra, S.
797 Habbig, J. Dotsch, R.U. Muller, J.C. Bruning, T. Persigehl, R.H. Giles, T. Benzing, B.
798 Schermer, and M.C. Liebau. 2018. Targeted deletion of the AAA-ATPase Ruvbl1 in
799 mice disrupts ciliary integrity and causes renal disease and hydrocephalus. *Exp Mol*
800 *Med*. 50:75.
801 Dawson, S.C., and S.A. House. 2010. Life with eight flagella: flagellar assembly and division in
802 Giardia. *Curr Opin Microbiol*. 13:480-490.
803 Desai, P.B., A.B. Dean, and D.R. Mitchell. 2018. Cytoplasmic preassembly and trafficking of
804 axonemal dyneins. *In* Dyneins. 140-161.
805 Diop, S.B., K. Bertaux, D. Vasanthi, A. Sarkeshik, B. Goirand, D. Aragnol, N.S. Tolwinski, M.D.
806 Cole, J. Pradel, J.R. Yates, 3rd, R.K. Mishra, Y. Graba, and A.J. Saurin. 2008. Reptin and
807 Pontin function antagonistically with PcG and TrxG complexes to mediate Hox gene
808 control. *EMBO Rep*. 9:260-266.
809 Fabczak, H., and A. Osinka. 2019. Role of the Novel Hsp90 Co-Chaperones in Dynein Arms'
810 Preassembly. *Int J Mol Sci*. 20.
811 Fabian, L., and J.A. Brill. 2012. Drosophila spermiogenesis: Big things come from little
812 packages. *Spermatogenesis*. 2:197-212.
813 Fatima, R. 2011. Drosophila Dynein intermediate chain gene, Dic61B, is required for
814 spermatogenesis. *PLoS One*. 6:e27822.
815 Fawcett, D.W., E.M. Eddy, and D.M. Phillips. 1970. Observations on the fine structure and
816 relationships of the chromatoid body in mammalian spermatogenesis. *Biol Reprod*.
817 2:129-153.
818 Fingerhut, J.M., J.V. Moran, and Y.M. Yamashita. 2019. Satellite DNA-containing gigantic
819 introns in a unique gene expression program during Drosophila spermatogenesis.
820 *PLoS Genet*. 15:e1008028.
821 Fowkes, M.E., and D.R. Mitchell. 1998. The role of preassembled cytoplasmic complexes in
822 assembly of flagellar dynein subunits. *Mol Biol Cell*. 9:2337-2347.
823 Fuller, M.T. 1993. Spermatogenesis. *In* The Development of Drosophila Melanogaster. Vol. 1.
824 M. Bate, Arias, A.M., editor. Cold Spring Harbor Laboratory Press, New York. 71-148.
825 Glock, C., M. Heumuller, and E.M. Schuman. 2017. mRNA transport & local translation in
826 neurons. *Curr Opin Neurobiol*. 45:169-177.
827 Goldstein, L.S., R.W. Hardy, and D.L. Lindsley. 1982. Structural genes on the Y chromosome
828 of Drosophila melanogaster. *Proc Natl Acad Sci U S A*. 79:7405-7409.

829 Gorynia, S., T.M. Bandeiras, F.G. Pinho, C.E. McVey, C. Vonrhein, A. Round, D.I. Svergun, P.
830 Donner, P.M. Matias, and M.A. Carrondo. 2011. Structural and functional insights into
831 a dodecameric molecular machine - the RuvBL1/RuvBL2 complex. *J Struct Biol*.
832 176:279-291.
833 Gottardo, M., G. Callaini, and M.G. Riparbelli. 2013. The cilium-like region of the Drosophila
834 spermatocyte: an emerging flagellum? *J Cell Sci*. 126:5441-5452.
835 Hales, K.G., and M.T. Fuller. 1997. Developmentally regulated mitochondrial fusion mediated
836 by a conserved, novel, predicted GTPase. *Cell*. 90:121-129.
837 Han, Y.G., B.H. Kwok, and M.J. Kernan. 2003. Intraflagellar transport is required in Drosophila
838 to differentiate sensory cilia but not sperm. *Curr Biol*. 13:1679-1686.
839 Hardy, R.W., K.T. Tokuyasu, and D.L. Lindsley. 1981. Analysis of spermatogenesis in
840 Drosophila melanogaster bearing deletions for Y-chromosome fertility genes.
841 *Chromosoma*. 83:593-617.
842 Hime, G.R., J.A. Brill, and M.T. Fuller. 1996. Assembly of ring canals in the male germ line from
843 structural components of the contractile ring. *J Cell Sci*. 109 (Pt 12):2779-2788.
844 Hoeng, J.C., S.C. Dawson, S.A. House, M.S. Sagolla, J.K. Pham, J.J. Mancuso, J. Lowe, and W.Z.
845 Cande. 2008. High-resolution crystal structure and in vivo function of a kinesin-2
846 homologue in Giardia intestinalis. *Mol Biol Cell*. 19:3124-3137.
847 Huen, J., Y. Kakihara, F. Ugwu, K.L. Cheung, J. Ortega, and W.A. Houry. 2010. Rvb1-Rvb2:
848 essential ATP-dependent helicases for critical complexes. *Biochem Cell Biol*. 88:29-40.
849 Huizar, R.L., C. Lee, A.A. Boulgakov, A. Horani, F. Tu, E.M. Marcotte, S.L. Brody, and J.B.
850 Wallingford. 2018. A liquid-like organelle at the root of motile ciliopathy. *Elife*. 7.
851 Ishikawa, H., and W.F. Marshall. 2011. Ciliogenesis: building the cell's antenna. *Nat Rev Mol*
852 *Cell Biol*. 12:222-234.
853 Jain, S., J.R. Wheeler, R.W. Walters, A. Agrawal, A. Barsic, and R. Parker. 2016. ATPase-
854 Modulated Stress Granules Contain a Diverse Proteome and Substructure. *Cell*.
855 164:487-498.
856 Kakihara, Y., and M. Saeki. 2014. The R2TP chaperone complex: its involvement in snoRNP
857 assembly and tumorigenesis. *Biomol Concepts*. 5:513-520.
858 Kee, H.L., J.F. Dishinger, T.L. Blasius, C.J. Liu, B. Margolis, and K.J. Verhey. 2012. A size-
859 exclusion permeability barrier and nucleoporins characterize a ciliary pore complex
860 that regulates transport into cilia. *Nat Cell Biol*. 14:431-437.
861 Kwitny, S., A.V. Klaus, and G.R. Hunnicutt. 2010. The annulus of the mouse sperm tail is
862 required to establish a membrane diffusion barrier that is engaged during the late
863 steps of spermiogenesis. *Biol Reprod*. 82:669-678.
864 Lee, C.S., A. Putnam, T. Lu, S. He, J.P.T. Ouyang, and G. Seydoux. 2020. Recruitment of mRNAs
865 to P granules by condensation with intrinsically-disordered proteins. *Elife*. 9.
866 Li, Y., L. Zhao, S. Yuan, J. Zhang, and Z. Sun. 2017. Axonemal dynein assembly requires the
867 R2TP complex component Pontin. *Development*. 144:4684-4693.
868 Lin, Y.C., P. Niewiadomski, B. Lin, H. Nakamura, S.C. Phua, J. Jiao, A. Levchenko, T. Inoue, R.
869 Rohatgi, and T. Inoue. 2013. Chemically inducible diffusion trap at cilia reveals
870 molecular sieve-like barrier. *Nat Chem Biol*. 9:437-443.
871 Liu, G., L. Wang, and J. Pan. 2019. Chlamydomonas WDR92 in association with R2TP-like
872 complex and multiple DNAAFs to regulate ciliary dynein preassembly. *J Mol Cell Biol*.
873 11:770-780.

874 Mao, Y.Q., and W.A. Houry. 2017. The Role of Pontin and Reptin in Cellular Physiology and
875 Cancer Etiology. *Front Mol Biosci*. 4:58.
876 Medioni, C., K. Mowry, and F. Besse. 2012. Principles and roles of mRNA localization in animal
877 development. *Development*. 139:3263-3276.
878 Muller, H.A. 2008. Immunolabeling of embryos. *Methods Mol Biol*. 420:207-218.
879 Noguchi, T., M. Koizumi, and S. Hayashi. 2011. Sustained elongation of sperm tail promoted
880 by local remodeling of giant mitochondria in Drosophila. *Curr Biol*. 21:805-814.
881 Olivieri, G., and A. Olivieri. 1965. Autoradiographic study of nucleic acid synthesis during
882 spermatogenesis in Drosophila melanogaster. *Mutat Res*. 2:366-380.
883 Phillips, D.M. 1970. Insect sperm: their structure and morphogenesis. *J Cell Biol*. 44:243-277.
884 Puchades, C., C.R. Sandate, and G.C. Lander. 2020. The molecular principles governing the
885 activity and functional diversity of AAA+ proteins. *Nat Rev Mol Cell Biol*. 21:43-58.
886 Rebollo, E., S. Llamazares, J. Reina, and C. Gonzalez. 2004. Contribution of noncentrosomal
887 microtubules to spindle assembly in Drosophila spermatocytes. *PLoS Biol*. 2:E8.
888 Reiter, J.F., O.E. Blacque, and M.R. Leroux. 2012. The base of the cilium: roles for transition
889 fibres and the transition zone in ciliary formation, maintenance and
890 compartmentalization. *EMBO Rep*. 13:608-618.
891 Riparbelli, M.G., G. Callaini, and T.L. Megraw. 2012. Assembly and persistence of primary cilia
892 in dividing Drosophila spermatocytes. *Dev Cell*. 23:425-432.
893 Rivera-Calzada, A., M. Pal, H. Munoz-Hernandez, J.R. Luque-Ortega, D. Gil-Carton, G.
894 Degliesposti, J.M. Skehel, C. Prodromou, L.H. Pearl, and O. Llorca. 2017. The Structure
895 of the R2TP Complex Defines a Platform for Recruiting Diverse Client Proteins to the
896 HSP90 Molecular Chaperone System. *Structure*. 25:1145-1152 e1144.
897 Robinson, S.W., P. Herzyk, J.A. Dow, and D.P. Leader. 2013. FlyAtlas: database of gene
898 expression in the tissues of Drosophila melanogaster. *Nucleic Acids Res*. 41:D744-750.
899 Rosenbaum, J.L., and G.B. Witman. 2002. Intraflagellar transport. *Nat Rev Mol Cell Biol*. 3:813-
900 825.
901 Sarpal, R., S.V. Todi, E. Sivan-Loukianova, S. Shirolikar, N. Subramanian, E.C. Raff, J.W.
902 Erickson, K. Ray, and D.F. Eberl. 2003. Drosophila KAP interacts with the kinesin II
903 motor subunit KLP64D to assemble chordotonal sensory cilia, but not sperm tails.
904 *Curr Biol*. 13:1687-1696.
905 Sinden, R.E., E.U. Canning, and B. Spain. 1976. Gametogenesis and fertilization in Plasmodium
906 yoelii nigeriensis: a transmission electron microscope study. *Proc R Soc Lond B Biol*
907 *Sci*. 193:55-76.
908 Sinden, R.E., A. Talman, S.R. Marques, M.N. Wass, and M.J. Sternberg. 2010. The flagellum in
909 malarial parasites. *Curr Opin Microbiol*. 13:491-500.
910 Stolc, V., M.P. Samanta, W. Tongprasit, and W.F. Marshall. 2005. Genome-wide transcriptional
911 analysis of flagellar regeneration in Chlamydomonas reinhardtii identifies orthologs
912 of ciliary disease genes. *Proc Natl Acad Sci U S A*. 102:3703-3707.
913 Tammana, D., and T.V.S. Tammana. 2017. Human DNA helicase, RuvBL1 and its
914 Chlamydomonas homologue, CrRuvBL1 plays an important role in ciliogenesis.
915 *Cytoskeleton (Hoboken)*. 74:251-259.
916 Tates, A.D. 1971. Cytodifferentiation during spermatogenesis in Drosophila melanogaster:
917 An electon microsope study. Vol. Ph.D., Rijksuniversiteit, Leiden.
918 Tokuyasu, K.T. 1975. Dynamics of spermiogenesis in Drosophila melanogaster. VI.
919 Significance of "onion" nebenkern formation. *J Ultrastruct Res*. 53:93-112.

Trcek, T., M. Grosch, A. York, H. Shroff, T. Lionnet, and R. Lehmann. 2015. Drosophila germ granules are structured and contain homotypic mRNA clusters. *Nat Commun*. 6:7962.

Venteicher, A.S., Z. Meng, P.J. Mason, T.D. Veenstra, and S.E. Artandi. 2008. Identification of ATPases pontin and reptin as telomerase components essential for holoenzyme assembly. *Cell*. 132:945-957.

Vieillard, J., M. Paschaki, J.L. Duteyrat, C. Augiere, E. Cortier, J.A. Lapart, J. Thomas, and B. Durand. 2016. Transition zone assembly and its contribution to axoneme formation in Drosophila male germ cells. *J Cell Biol*. 214:875-889.

Wang, J.T., J. Smith, B.C. Chen, H. Schmidt, D. Rasoloson, A. Paix, B.G. Lambrus, D. Calidas, E. Betzig, and G. Seydoux. 2014. Regulation of RNA granule dynamics by phosphorylation of serine-rich, intrinsically disordered proteins in C. elegans. *Elife*. 3:e04591.

Wang, Y., R. Xu, Y. Cheng, H. Cao, Z. Wang, T. Zhu, J. Jiang, H. Zhang, C. Wang, L. Qi, M. Liu, X. Guo, J. Huang, and J. Sha. 2019. RSBP15 interacts with and stabilizes dRSPH3 during sperm axoneme assembly in Drosophila. *J Genet Genomics*. 46:281-290.

Wheway, G., L. Nazlamova, and J.T. Hancock. 2018. Signaling through the Primary Cilium. *Front Cell Dev Biol*. 6:8.

Yamaguchi, H., T. Oda, M. Kikkawa, and H. Takeda. 2018. Systematic studies of all PIH proteins in zebrafish reveal their distinct roles in axonemal dynein assembly. *Elife*. 7.

Zhao, L., S. Yuan, Y. Cao, S. Kallakuri, Y. Li, N. Kishimoto, L. DiBella, and Z. Sun. 2013. Reptin/Ruvbl2 is a Lrrc6/Seahorse interactor essential for cilia motility. *Proc Natl Acad Sci U S A*. 110:12697-12702.

Zur Lage, P., F.G. Newton, and A.P. Jarman. 2019. Survey of the Ciliary Motility Machinery of Drosophila Sperm and Ciliated Mechanosensory Neurons Reveals Unexpected Cell-Type Specific Variations: A Model for Motile Ciliopathies. *Front Genet*. 10:24.

Zur Lage, P., P. Stefanopoulou, K. Styczynska-Soczka, N. Quinn, G. Mali, A. von Kriegsheim, P. Mill, and A.P. Jarman. 2018. Ciliary dynein motor preassembly is regulated by Wdr92 in association with HSP90 co-chaperone, R2TP. *J Cell Biol*. 217:2583-2598.